remote sensing

MDPI

Article

Spatiotemporal Variations in Near-Surface Soil Water Content across Agroecological Regions of Mainland India: 1979–2022 (44 Years)

Alka Rani [1], Nishant K. Sinha [1], Bikram Jyoti [2], Jitendra Kumar [1], Dhiraj Kumar [1], Rahul Mishra [1], Pragya Singh [3], Monoranjan Mohanty [1], Somasundaram Jayaraman [1], Ranjeet Singh Chaudhary [1], Narendra Kumar Lenka [1], Nikul Kumari [4] and Ankur Srivastava [4,*]

[1] Division of Soil Physics, ICAR-Indian Institute of Soil Science, Nabibagh, Berasia Road, Bhopal 462038, India; alka.rani1@icar.gov.in (A.R.); nishant.sinha@icar.gov.in (N.K.S.); jitendra.kumar1@icar.gov.in (J.K.); dhiraj.kumar@icar.gov.in (D.K.); rahul.mishra@icar.gov.in (R.M.); monoranjan.mohanty@icar.gov.in (M.M.); somasundaram.j@icar.gov.in (S.J.); ranjeet.chaudhary@icar.gov.in (R.S.C.); narendra.lenka@icar.gov.in (N.K.L.)

[2] ICAR-Central Institute of Agricultural Engineering, Nabibagh, Berasia Road, Bhopal 462038, India; bikram.jyoti@icar.gov.in

[3] ICAR-Indian Agricultural Research Institute, New Delhi 110012, India; prgsingh10@gmail.com

[4] Faculty of Science, University of Technology Sydney, Sydney, NSW 2007, Australia; nikulkumari258@gmail.com

* Correspondence: ankur.srivastava@uts.edu.au or ankursrivastava117@gmail.com

Abstract: This study was undertaken to address how near-surface soil water content (SWC) patterns have varied across diverse agroecological regions (AERs) of mainland India from 1979 to 2022 (44 years) and how these variations relate to environmental factors. Grid-wise trend analysis using the Mann–Kendall (MK) trend test and Sen's slope was conducted to determine the trends and their magnitudes. Additionally, we used Spearman's rank correlation (ρ) to explore the relationships of ESA CCI's near-surface SWC data with key environmental variables, including rainfall, temperature, actual evapotranspiration, and the normalized difference vegetation index (NDVI). The results revealed significant variations in SWC patterns and trends across different AERs and months. The MK trend test indicated that 17.96% of the area exhibited a significantly increasing trend ($p < 0.1$), while7.6% showed a significantly decreasing trend, with an average annual Sen's slope of 0.9×10^{-4} m^3 m^{-3} $year^{-1}$ for mainland India. Areas with the highest decreasing trends were AER-16 (warm per-humid with brown and red hill soils), AER-15 (hot subhumid to humid with alluvium-derived soils), and AER-17 (warm per-humid with red and lateritic soils). In contrast, increasing trends were the most prominent in AER-5 (hot semi-arid with medium and deep black soils), AER-6 (hot semi-arid with shallow and medium black soils), and AER-19 (hot humid per-humid with red, lateritic, and alluvium-derived soils). Significant increasing trends were more prevalent during monsoon and post-monsoon months while decreasing trends were noted in pre-monsoon months. Correlation analysis showed strong positive correlations of SWC with rainfall (ρ = 0.70), actual evapotranspiration (ρ = 0.74), and NDVI (ρ = 0.65), but weak or negative correlations with temperature (ρ = 0.12). This study provides valuable insights for policymakers to delineate areas based on soil moisture availability patterns across seasons, aiding in agricultural and water resource planning under changing climatic conditions.

Keywords: agroecological regions; climate change; ESA CCI soil water content; Mann–Kendall trend; Sen's slope; Spearman's rank correlation

Citation: Rani, A.; Sinha, N.K.; Jyoti, B.; Kumar, J.; Kumar, D.; Mishra, R.; Singh, P.; Mohanty, M.; Jayaraman, S.; Chaudhary, R.S.; et al. Spatiotemporal Variations in Near-Surface Soil Water Content across Agroecological Regions of Mainland India: 1979–2022 (44 Years). *Remote Sens.* **2024**, *16*, 3108. https://doi.org/10.3390/rs16163108

Academic Editor: Dusan Gleich

Received: 18 July 2024
Revised: 13 August 2024
Accepted: 19 August 2024
Published: 22 August 2024

1. Introduction

Soil moisture is an important factor affecting agricultural productivity, hydrological cycles, and the sustainability of ecosystems. It serves as a vital link between the atmosphere

and the land, influencing plant growth, groundwater replenishment, and surface runoff. Grasping the spatial and temporal patterns of near-surface soil water content (SWC) is vital for managing water resources efficiently, planning agricultural activities, and addressing the impacts of climate variability [1]. Investigating the impacts of climate change on ecological systems, with a particular emphasis on hydrological resources, is a crucial area of study that scientists must prioritize. The occurrence of notable climate variations has been documented since around 1950, and the modification has been ascribed to the release of greenhouse gases (GHG) resulting from human activities [2]. As per Assessment Report 5 (AR5) [2], the earth's average temperature is projected to increase by as much as 4 °C by the year 2100. In recent decades, India has experienced a warming trend, which is consistent with global warming patterns [3]. An increase in temperature and rainfall patterns can have long-lasting consequences, potentially disrupting the availability of surface and underground water resources [4]. The fluctuations in precipitation, temperature, and evapotranspiration have significantly impacted the hydrological cycle, stream flow, and the corresponding water requirements of different sectors [5,6].

India's diverse climatic zones and varied topography pose a distinctive challenge when studying soil moisture patterns. The country encompasses agroecological regions (AERs) that span from arid deserts in Rajasthan to tropical monsoon areas in Kerala and temperate zones in the northern Himalayas. Different AERs are defined on the basis of climate, landform, soils, and/or land cover, and, therefore, encompass temperature and rainfall variability. Each of these regions features unique soil types, vegetation, and agricultural methods, all impacting SWC in distinct ways [7]. A recent study on the Narmada River in India investigated the impacts of long-term changes in precipitation and evapotranspiration [8]. Several studies have been conducted to assess the influence of climatic fluctuations on yearly and seasonal precipitation patterns and their intensity [9–11], the frequency of rainy days in diverse regions of India, and temperature trends [12–16]. The alterations in climatic parameters have a substantial impact on the country's overall economic condition and pose a challenge to the effective management of water resources and agricultural activities [17,18].

Consequently, there is a significant focus on conducting thorough investigations into the analysis of long-term trends pertaining to hydrologic variables such as SWC. This involves utilizing climatic data to examine the potential effects of climate variability on the hydrological cycle. Understanding the dynamics of surface soil moisture on a regional level is crucial for various applications, such as hydrological modeling, weather forecasting, and predicting crop yields [19,20]. Therefore, it is essential to accurately quantify surface soil moisture on a regional scale. While the gravimetric method is an accurate technique for measuring SWC, it is not feasible for large-scale monitoring [21,22]. Many networks worldwide use sensor-based techniques to monitor soil moisture continuously, but these measurements are limited to field or plot scale due to high maintenance costs for large-density networks at the regional level [23,24].

One way to determine regional soil moisture patterns is by utilizing data from global networks like Global Navigation Satellite System reflectometry (https://www.space4water.org/, accessed on 15 June 2024). Another option is obtaining soil moisture at a larger spatial scale through remote sensing and land surface models. However, studies have shown that these methods have varying levels of accuracy and uncertainty, as demonstrated by Entekhabi et al. [25], Kerr et al. [26], Mohanty et al. [27], and Wagner et al. [28]. The acquisition of SWC data has been facilitated by multiple platforms in recent years [29]. Notable among these are the European Space Agency Climate Change Initiative's (ESA CCI) multi-satellite soil moisture (SM), the Global Land Data Assimilation System (GLDAS) land surface models' simulated SM, and ERA-Interim reanalysis data. These products have undergone validation at various locations across the globe using observed SWC and have been employed in studies examining spatial-temporal SWC variations, hydrometeorology, and crop modeling [30–32]. However, significant uncertainties persist in surface soil moisture measurements, particularly in tropical

and subtropical regions [1], and the potential applications of these products in the Indian context remain largely unexplored.

It is important to note that simulated (GLDAS) and reanalysis (ERA5) SWC products carry model-dependent uncertainties, whereas satellite observations (ESA CCI) are free from such errors. While several satellites, including SMOS (Soil Moisture and Ocean Salinity), SMAP (Soil Moisture Active Passive), and ASCAT (Advanced Scatterometer), provide near-surface SWC data, their records only extend back to 2007, limiting their utility for long-term trend analysis. In contrast, the ESA CCI soil moisture product offers a distinct advantage for trend studies. By integrating observations from multiple satellites, it provides near-surface SWC data dating back to November 1979. This extended temporal coverage makes the ESA CCI product particularly suitable for analyzing long-term trends in soil moisture dynamics. Moreover, Agrawal and Chakraborty [33] found good agreement of ESACCI SM data with in-situ soil moisture observations over India. Several studies have been carried out to investigate the SWC trend, both on global [34,35] and regional scales [36–38]. However, the SWC trend analyses are highly sensitive to the study period and spatial scale, especially when monotonic approaches are followed [38].

For trend analysis, researchers can employ either parametric methods or nonparametric tests [39], each with its own strengths and limitations. Nonparametric methods are often preferred for trend analysis due to their fewer assumptions compared with parametric tests as failing to meet the latter's stricter requirements can lead to unreliable results, especially when dealing with environmental data. Since most of the hydrometeorological data are not normally distributed [40], a nonparametric distribution-free statistical method such as Sen's slope method [41] may be employed to determine the trend magnitude and its statistical significance by the MK test [42,43]. A combined approach, along with equations and procedures for the MK test statistic and Sen's estimator, is also explained by Bandyopadhyay et al. [44] and Subash et al. [45].

Despite various studies on SWC in India [32,46], none have utilized satellite-derived soil moisture products to determine SWC trends nationwide. There is a need to examine how near-surface SWC has changed over the past four decades across different AERs of India and how it is spatiotemporally associated with environmental variables such as rainfall, temperature, evapotranspiration, and vegetation status. This study was undertaken to answer these specific research questions. The significance of this research study lies in its comprehensive analysis of SWC trends across India's diverse AERs over a 44-year period (1979–2022). By revealing spatial and temporal patterns of soil moisture and their relationships with climate variables, this study provides crucial insights for sustainable water resource management, agricultural planning, and climate change adaptation strategies.

2. Materials and Methods

2.1. Study Area

India is a vast country located in South Asia, extending from 8°4′N to 37°6′N latitudes and 68°7′E to 97°25′E longitudes. India has an area of approximately 328.7 million hectares, with gross and net cultivated areas of 200.2 and 139.4 million hectares, respectively [47]. Administratively, India is divided into 28 states and 8 union territories. India has varied topography, from the Himalayan Mountains in the northern and northeastern regions to the fertile Indo-Gangetic plains. The Thar Desert is present in the northwestern region. The peninsular plateau extends from the central to the southern parts of India where the Eastern and Western Ghats surround the southern coastlines. Mainland India is surrounded by the Bay of Bengal, the Arabian Sea, and the Indian Ocean at the eastern, western, and southern coastlines. Andaman and Nicobar Islands are situated in the Bay of Bengal, whereas Lakshadweep Islands are in the Arabian Sea. India has a broadly tropical monsoon-type climate. As per India Meteorological Department (IMD), India has four meteorological seasons, i.e., winter (January–February), summer or pre-monsoon (March–May), monsoon (June–September), and autumn or post-monsoon (October–December). The Southwest monsoon provides rainfall to most parts of India during the months of June to September,

whereas some portions of South India, like Tamil Nadu and Kerala, also receive rainfall from the Northeast monsoon from October to December. The failure of the monsoon or inadequate rainfall during the monsoon, variability in rainfall distribution, and the delayed onset or break in the monsoon can cause drought, whereas the excess and high-intensity rainfall leads to flash floods in some areas. The frequency of droughts and floods is expected to increase in India due to climate change [48]. The net irrigated area has increased from 18% in 1951 to 52% in 2021 due to government interventions [49,50]. The states of Punjab, Haryana, Uttar Pradesh, and Bihar have more than 70% of the area under irrigated agriculture, while the northeastern states—Chhattisgarh, Jharkhand, Goa, Himachal Pradesh, Karnataka, Kerala, Maharashtra, and Orissa—have less than 40% of the area under irrigated agriculture [50]. According to the National Bureau of Soil Survey and Land Use Planning (NBSS&LUP), India is divided into 20 AERs based on physiography, climate, length of growing period (LGP), and soil type (Figure 1). Each AER has similar suitability and constraints for agricultural production and is effective for the transfer of agro-technology. The details of these AERs are given by Gajbhiye and Mandal [51] and are briefly discussed in Table 1. In our study, we focused exclusively on the AERs of mainland India, excluding the Andaman and Nicobar Islands and the Lakshadweep Islands, which are part of AER-20. This exclusion is due to their relatively small and dispersed areas, as well as the lack of reliable data for these regions.

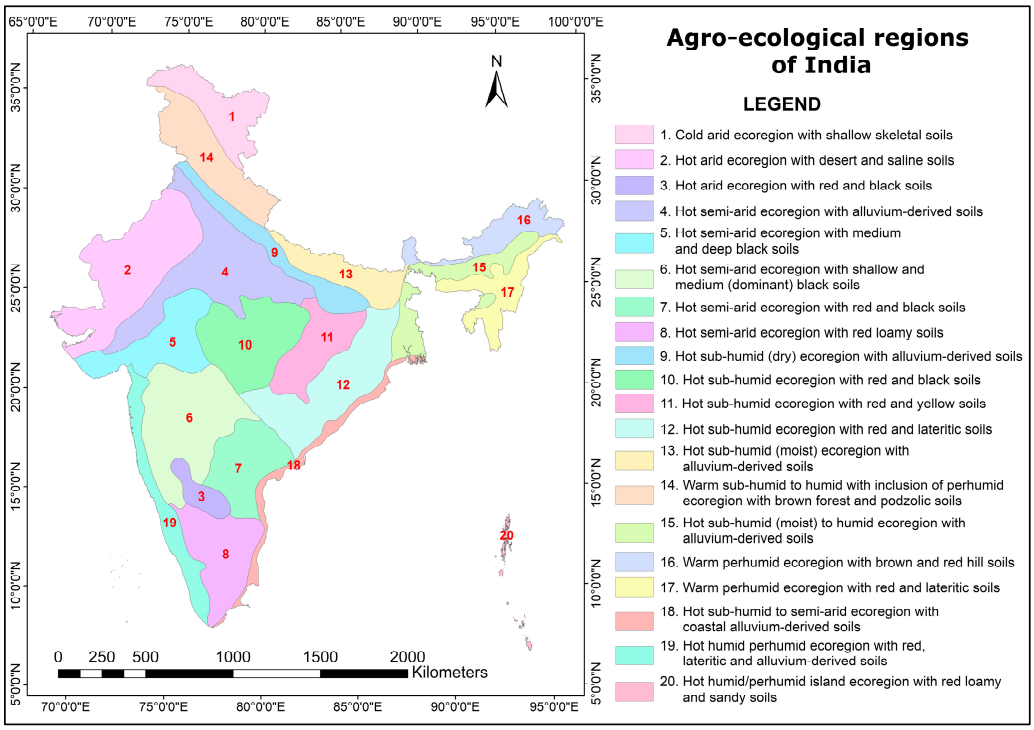

Figure 1. Map of agroecological regions of India (Source: National Bureau of Soil Survey and Land Use Planning, India).

Table 1. Characteristics of different agroecological regions (AERs) of India.

AER No.	Agroecological Region	Geographical Distribution	Brief Characteristics	Major Crops
AER-1	Cold arid ecoregion with shallow skeletal soils	Northwestern Himalayan region covering Ladakh and Gilgit districts	Mild summers and severe winters with a mean annual temperature of less than 8 °C and a mean annual rainfall of less than 15 cm, acidic soil moisture, and cryic soil temperature regime, and an LGP < 90 days	Vegetables, millet, and fodder

Table 1. *Cont.*

AER No.	Agroecological Region	Geographical Distribution	Brief Characteristics	Major Crops
AER-2	Hot arid ecoregion with desert and saline soils	Western plain comprising Kachchh and part of the Kathiawar Peninsula	Hot summers and cool winters with mean annual rainfall less than 40 cm, LGP < 90 days, aridic soil moisture, and a hyperthermic soil temperature regime	Pearl millet and fodder
AER-3	Hot arid ecoregion with red and black soils	Some parts of the Deccan Plateau	Hot and dry summers and mild winters with mean annual rainfall ranging from 40 to 50 cm, LGP < 90 days, aridic-ustic soil moisture, and isohyperthermic soil temperature regimes	Pearl millet, sorghum, and safflower
AER-4	Hot semi-arid ecoregion with alluvium-derived soils	Some areas of Gujarat, the northern plains and the Central Highlands	Hot and dry summers and cool winters with annual rainfall ranging from 50 to 100 cm, LGP ranging from 90 to 150 days, typic ustic soil moisture, and a hyperthermic soil temperature regime	Wheat, paddy, maize, and pulses
AER-5	Hot semi-arid ecoregion with medium and deep black soils	Some areas of the Central Highlands (Malwa), Gujarat Plains and Kathiawar peninsula, western Madhya Pradesh, southeastern Rajasthan and Gujarat	Hot and wet summer and dry winter with annual rainfall ranging from 50 to 100 cm, LGP ranging from 90 to 150 days, typic ustic soil moisture, and hyperthermic and isohyperthermic soil temperature regimes	Sorghum, pearl millet, pigeon pea, groundnut, soybeans, maize, pulses, and wheat
AER-6	Hot semi-arid ecoregion with shallow and medium (dominant) black soils	Some parts of the Deccan Plateau	Hot and humid summers and mild and dry winters with annual rainfall ranging from 60 to 100 cm, LGP of 90–150 days, loamy and clayey soils with ustic soil moisture, and isohyperthermic soil temperature regimes	Sorghum, pigeon pea, pearl millet, safflower, sunflower, cotton, and groundnut
AER-7	Hot semi-arid ecoregion with red and black soils	Some parts of the Deccan Plateau (Telangana) and Eastern Ghats of Andhra Pradesh	Hot and moist summers and mild and dry winters with an annual rainfall of 60–110 cm, LGP of 90–150 days, ustic soil moisture, and isohyperthermic soil temperature regimes	Sorghum, cotton, pigeon pea, paddy, groundnut, castor, sunflower, safflower, and oilseeds
AER-8	Hot semi-arid ecoregion with red loamy soils	Some parts of the Eastern Ghats, southern parts of the Deccan Plateau, Tamil Nadu Uplands, and western Karnataka	Hot and dry summer and mild winter with an annual rainfall of 60–100 cm, LGP of 90–150 days, ustic soil moisture, and isohyperthermic soil temperature regimes	Millet, pulses, groundnut, sorghum, safflower, paddy, sugarcane, and cotton
AER-9	Hot subhumid (dry) ecoregion with alluvium-derived soils	Northern Indo-Gangetic Plains	Hot summers and cool winters with an annual rainfall of 100–120 cm, LGP of 150–180 days, deep and loamy alluvial soils with ustic soil moisture, and a hyperthermic soil temperature regime	Paddy, maize, barley, pigeon pea, jute, wheat, mustard, lentil, sugarcane, and cotton
AER-10	Hot subhumid ecoregion with red and black soils	Malwa Plateau and Bundelkhand Uplands of the Central Highlands	Hot summers and mild winters with an annual rainfall of 100–150 cm, LGP of 150–180 days, deep black soils interspersed with patches of red soils with typic ustic soil moisture, and hyperthermic soil temperature regimes	Paddy, sorghum, pigeon pea, soybean, gram, wheat, and vegetables
AER-11	Hot subhumid ecoregion with red and yellow soils	Chhattisgarh region of the eastern plateau	Hot summers and cool winters with an annual rainfall of 120–160 cm, LGP of 150–180 days, deep loamy, non-calcareous, neutral to slightly acidic soils, ustic soil moisture, and hyperthermic soil temperature regimes	Paddy, millet, pulses, and wheat

Table 1. *Cont.*

AER No.	Agroecological Region	Geographical Distribution	Brief Characteristics	Major Crops
AER-12	Hot subhumid ecoregion with red and lateritic soils	Some parts of the Chhota Nagpur region of the Eastern Plains and Eastern Ghats	Hot summers and cool winters with an annual rainfall of 100–160 cm, LGP of 150–210 days, fine loamy to clayey, non-calcareous, slightly to moderately acidic soils with low cation exchange capacity, typic ustic soil moisture, and hyperthermic soil temperature regimes	Paddy, pulses, groundnut, and wheat
AER-13	Hot subhumid (moist) ecoregion with alluvium-derived soils	Some parts of the Eastern Plains	Hot, wet summers and cool, dry winters with an annual rainfall of 140–180 cm, LGP of 180–210 days, gently sloping alluvium-derived soils, udic and ustic soil moisture regimes, and a hyperthermic soil temperature regime	Paddy, wheat, maize, pulses, groundnut, sugarcane, and vegetables
AER-14	Warm subhumid to humid with the inclusion of a per-humid ecoregion with brown forest and podzolic soils	Western Himalayas	Mild summers and cold winters with an annual rainfall of 100–200 cm, brown forest and podzolic soils, and udic or udic-ustic soil moisture regimes	Wheat, millet, maize, paddy, and apples
AER-15	Hot subhumid (moist) to humid ecoregion with alluvium-derived soils	Bengal Basin and Assam Plain	Hot summers and mild to moderately cool winters with an annual rainfall of 140–160 cm in the Ganga Plain and 180–200 cm in Tripura and Teesta-Brahmaputra Plains, LGP greater than 210 days, slightly to strongly acidic soils with udic-ustic soil moisture and a hyperthermic soil temperature regime	Paddy, jute, pulses, oilseeds, tea, and horticultural crops like pineapple, citrus, and banana
AER-16	Warm per-humid ecoregion with brown and red hill soils	Some parts of the Eastern Himalayas	Warm summer and cool winter with an annual rainfall of more than 200 cm, LGP of more than 270 days, deep and organic matter-rich brown forest soils, and udic soil moisture regime, with soil temperature regimes varying from thermic, mesic to hyperthermic based on the elevation	Jhum or shifting cultivation with mixed crops like millet, potato, maize, paddy, mustard, sesamum, pulses, plantation, and horticultural crops
AER-17	Warm per-humid ecoregion with red and lateritic soils	Northeastern hills	Warm summers and cool winters with an annual rainfall of 200–300 cm, LGP of more than 270 days, shallow to very deep, loamy, red and lateritic and red and yellow soils, udic soil moisture regime, and hyperthermic to thermic soil temperature regimes based on topography	Jhum or shifting cultivation with paddy, millet, maize, jute, and potato, plantation, and horticultural crops
AER-18	Hot subhumid to semi-arid ecoregion with coastal alluvium-derived soils	Eastern Coastal Plains	Annual rainfall of 90–110 cm, most of which is received during October to December, LGP of 90–150 days, and an isohyperthermic soil temperature regime	Coconut, paddy, black gram, lentil, sunflower, and groundnut
AER-19	Hot humid per-humid ecoregion with red, lateritic, and alluvium-derived soils	Some parts of the Western Ghats and coastal plains	Hot and humid summers and warm winters with an annual rainfall of more than 200 cm, LGP of 150–210 days, red and lateritic soils with udic soil moisture, and an isohyperthermic soil temperature regime	Paddy, tapioca, coconut, and spices
AER-20	Hot humid/per-humid island ecoregion with red loamy and sandy soils	Andaman and Nicobar Islands, and Lakshadweep Islands	Tropical climate with little difference between mean summer and winter temperatures and annual rainfall ranging from 160 to 300 cm, LGP of more than 210 days, red loamy soils on Andaman and Nicobar Islands and calcareous and sandy soils on Lakshadweep Islands with udic soil moisture and an isohyperthermic soil temperature regime	Paddy, coconut, areca nut, and oil palm

2.2. Data

The European Space Agency's Climate Change Initiative for Soil Moisture (ESA CCI SM) project (https://www.esa-soilmoisture-cci.org/, accessed on 15 June 2024) provides multi-decadal, long-term, global, daily, satellite-derived surface volumetric soil moisture (0–5 cm depth) starting from November 1978 onward at 0.25° spatial resolution. The ESA CCI provides three types of soil moisture products, i.e., active, passive, and combined. The active product is produced from the observations of C-band scatterometers onboard ERS-1, ERS-2, MetOp-A, and MetOp-B satellites. The passive product is produced from the multifrequency radiometers from Nimbus 7 SMMR, DMSP SSM/I, TRMM TMI, Aqua AMSR-E, Coriolis WindSat, GCOM-W1 AMSR2, FengYun-3B/C/D MWRI, SMAP, and SMOS MIRAS sensors. The combined product is produced by the combination of both active and passive products depending on their relative sensitivity to vegetation density. The detailed algorithm for the development of this product is given by Gruber et al. [52]. Agrawal and Chakraborty [33] reported good agreement with the ESACCI SM dataset with in-situ soil moisture observations from 117 Continental Tropical Convergence Zone Programme stations spread across India, having relatively higher accuracy over the plains of northern and central India. In this study, the ESA CCI SM (version 8.1) combined product was used from 1979 to 2022 (44 years) as the combined product was reported to have higher accuracy compared with the other products [53,54]. The pixel-wise monthly average of near-surface SWC was computed using the daily data from the ESA CCI dataset spanning from January 1979 to December 2022, encompassing a total of 528 months.

For evaluating the effects of weather parameters such as rainfall and temperature on near-surface SWC, we obtained the gridded daily rainfall data at 0.25° resolution, and the minimum and maximum temperature data at 1° resolution from the IMD spanning the period from 1979 to 2022. The mean air temperature was computed by averaging the daily minimum and maximum temperatures. Monthly rainfall and air temperature were derived by summing the daily values and computing averages, respectively. To assess the relationship between SWC and vegetation dynamics, we acquired and processed actual evapotranspiration and Normalized Difference Vegetation Index (NDVI) data for mainland India. We used MODIS (Moderate Resolution Imaging Spectroradiometer) actual evapotranspiration data, available from 2000 onward at 500 m spatial resolution and 8-day temporal intervals. Monthly actual evapotranspiration was calculated by summing the corresponding 8-day data. Monthly NDVI data were obtained from AVHRR (Advanced Very High Resolution Radiometer) and MODIS, available from 1982 onward at 5 km spatial resolution. To ensure consistency across datasets, all data were resampled to a 0.25° spatial resolution, matching that of the ESA CCI SWC data. This resampling process allowed for direct comparison and analysis across all variables. Table 2 summarizes the satellite datasets used in this study, including their source, temporal coverage, original spatial resolution, and temporal frequency.

Table 2. Satellite datasets used in this study.

Input Parameter	Dataset Name	Data Source	Temporal Period	Spatial Resolution	Temporal Resolution
Near-surface SWC	ESA CCI SM (v 8.1)	https://www.esa-soilmoisture-cci.org/ (accessed on 15 June 2024)	1979 to 2022	0.25°	Daily
Rainfall	IMD gridded rainfall	IMD [55]	1979 to 2022	0.25°	Daily
Maximum temperature	IMD maximum temperature	IMD [56]	1979 to 2022	1°	Daily
Minimum temperature	IMD minimum temperature	IMD [56]	1979 to 2022	1°	Daily
Actual evapotranspiration	MODIS MOD16A2GF	NASA	2000 to 2022	500 m	8-day
NDVI	AVHRR and MODIS	https://zenodo.org/doi/10.5281/zenodo.4305974 (accessed on 15 June 2024)	1982 to 2019	5 km	Monthly
	MODIS MOD13C2	NASA	2020 to 2022	5 km	Monthly

2.3. Methods

2.3.1. Mann–Kendall Trend Test

The time series of SWC were analyzed using the Mann–Kendall (MK) trend test, and their magnitude was estimated through Sen's slope estimator. The MK trend test [42,43] is a nonparametric, rank-based correlation test used to detect monotonic upward or downward trends in time-series data. The MK test is easy to perform and is robust to the presence of outliers or missing data. The null hypothesis of the MK test is the absence of a trend, while the alternate hypothesis is the presence of a trend. In the MK test, each value in the time-series data is compared with the other values sequentially. The expression of the MK test (S) statistic is

$$S = \sum_{k=1}^{n-1} \sum_{j=k+1}^{n} sign(x_j - x_k) \quad (1)$$

where n is the length of time-series data, x_j and x_k are two sequential values of data. The function $sign(x_j - x_k)$ obtains the values as expressed below:

$$sign(x_j - x_k) = \begin{bmatrix} +1, & (x_j - x_k) > 0 \\ 0, & (x_j - x_k) = 0 \\ -1, & (x_j - x_k) < 0 \end{bmatrix} \quad (2)$$

$$Var(S) = \frac{n(n-1)(2n+5)}{18} \quad (3)$$

Here, *Var(S)* is the variance of the dataset. The Z-statistic is computed as follows:

$$Z - \text{statistic} = \begin{bmatrix} \frac{S-1}{\sqrt{Var(S)}}, & if\ S > 0 \\ 0, & if\ S = 0 \\ \frac{S+1}{\sqrt{Var(S)}}, & if\ S < 0 \end{bmatrix} \quad (4)$$

The positive value of standardized Z statistic denotes increasing trend, whereas the negative value denotes a decreasing trend. The Kendall Tau (τ) or Kendall rank correlation coefficient is computed as follows:

$$\tau = \frac{S}{D} \quad (5)$$

where D is the total number of pair combinations computed using the following equation:

$$D = \frac{n(n-1)}{2} \quad (6)$$

Kendall's Tau measures the monotony of the slope. Its value ranges from −1 to +1, where a positive value denotes an increasing trend, and a negative value denotes a decreasing trend. The magnitude of the slope of the trend or change in the variable per unit time of a trend is estimated using Sen's slope estimator [41]. Sen's slope is the median of all the slopes computed between each pair of points in the time series. Sen's slope is calculated using the following equation:

$$\text{Sen's slope} = \text{Median}\ \{(x_j - x_k)/(j - k)\},\ j > k \quad (7)$$

where x_j and x_k are the values of variables at time steps j and k, respectively.

The MK test was performed on the monthly time-series data of near-surface SWC ranging from 1979 to 2022 (44 years). Kendall's Tau and Sen's slope were computed for each pixel for a particular month and for a whole year. This method has been used for the time-series analysis of precipitation, temperature, soil water, and vegetation dynamics by several researchers [1,31,57–61]. For the computation of the MK test and Sen's slope over the raster dataset of SWC, 'raster' [62], 'Kendall' [63], and 'trend' [64] packages of R software v 4.2.0 were used. The analysis was conducted at a 10% level of significance ($p < 0.1$) so that the balance between Type I and Type II errors can be established given

the exploratory nature of our research as well as the complex and noisy nature of data. While the conventional 5% level is more stringent, the 10% level allows for the detection of weaker but potentially meaningful trends in our large-scale, long-term dataset. The use of a 10% significance level is supported by various researchers in ecological and environmental studies [65–67], particularly when dealing with complex natural systems where subtle trends may have important cumulative effects.

2.3.2. Spearman's Rank Correlation Test

To assess the relationships as well as similarity in the temporal patterns of the near-surface SWC with other environmental variables such as rainfall, temperature, actual evapotranspiration, and NDVI in different AERs of mainland India, the pixel-wise Spearman's rank correlation coefficient was computed using the 'raster' package [62] in R software v 4.2.0. The Spearman's rank correlation test, given by Spearman [68], is a nonparametric test to assess the strength and direction of the monotonic relationship between two datasets without assuming linearity or normal distribution of the variables. The Spearman's rank correlation coefficient (ρ) can be computed using the following formula:

$$\rho = 1 - \frac{6\sum d_i^2}{n(n^2-1)} \tag{8}$$

$$d_i = R(x_i) - R(y_i) \tag{9}$$

where d_i is the difference between the ranks of the 'i' observation of two variables x and y (denoted by $R(x_i)$ and $R(y_i)$), and n is the number of observations. The value of ρ ranges from -1 to +1, with values closer to ± 1 indicating stronger monotonic relationships. A positive ρ suggests that as one variable increases, the other tends to increase, while a negative ρ indicates an inverse relationship. Similar to the MK test, the correlation coefficients with p-values < 0.1 were considered as statistically significant. This test provides valuable insights into the relationships between near-surface SWC and key environmental variables across different AERs in mainland India. This test has been used by several researchers to assess the relationship of soil moisture with other variables [31,60,69,70]. Understanding these correlations is essential for elucidating the drivers of SWC variability and their implications for regional water management and agricultural practices.

3. Results

3.1. Spatial Variations of Near-Surface SWC

The spatial distribution of average annual near-surface SWC and its coefficient of variation (CV) for the 44-year period (1979–2022) are presented in Figure 2. Figure 3 illustrates the distribution of near-surface SWC data across different AERs using a boxplot, which displays the mean, median, interquartile range, and potential outliers for each region. Analysis of the data revealed significant spatial variability in SWC across different AERs of mainland India. The lowest average annual SWC was observed in AER-2 (0.15 m^3 m^{-3}), followed by AER-4 (0.18 m^3 m^{-3}). Conversely, the highest average annual SWC was recorded in AER-17 (0.30 m^3 m^{-3}), followed by AER-16 (0.28 m^3 m^{-3}) and AER-15 (0.27 m^3 m^{-3}). The CV of near-surface SWC across mainland India ranged from 1.93% to 57.28%, with an average of 28.90%. Spatial patterns in CV were evident, with AERs in northwestern, western, eastern, and central India with average CVs exceeding 30%. In contrast, northern, northeastern, and some parts of southern India showed lower variability, with CVs below 20% (Figure 2).

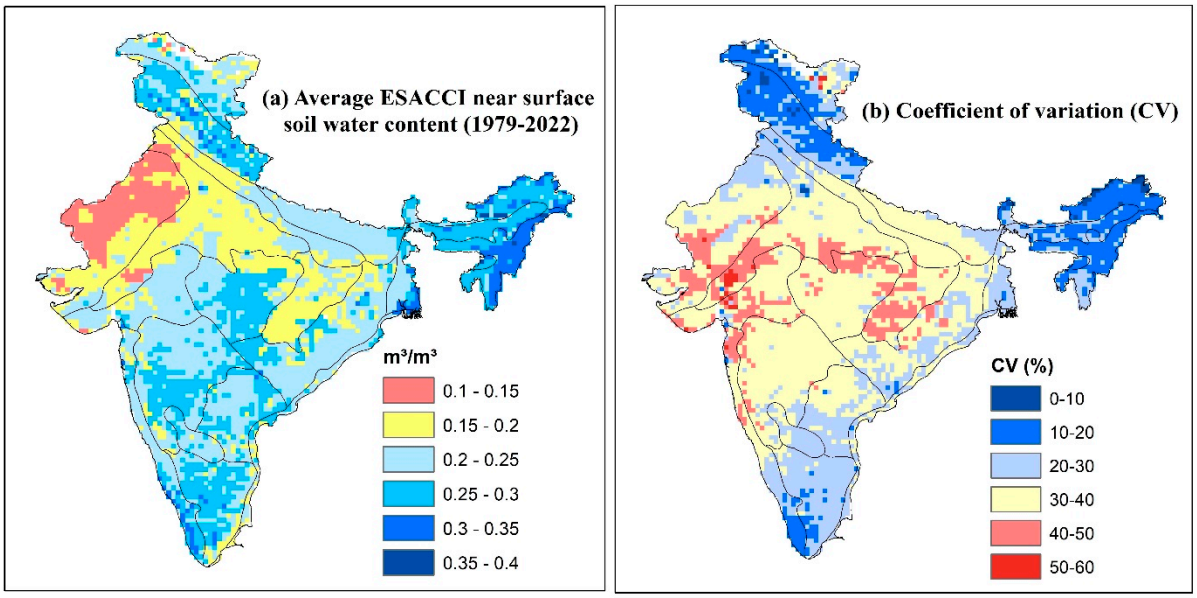

Figure 2. Spatial pattern of the (**a**) average annual near-surface SWC and (**b**) the coefficient of variation under different AERs of mainland India from 1979 to 2022 (44 years).

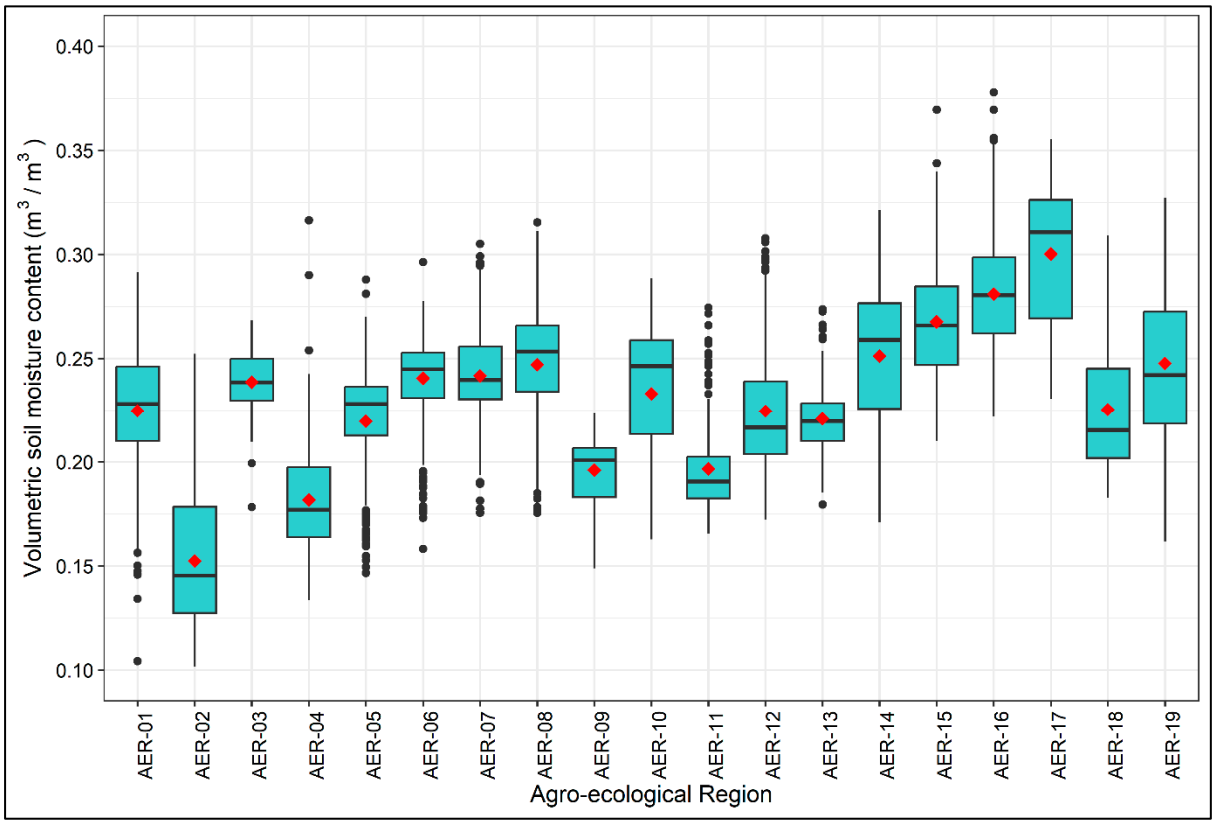

Figure 3. The boxplot of near-surface SWC across different AERs of mainland India. The red dot represents the mean value.

The monthly mean of the ESA CCI near-surface SWC for the 44-year period from 1979 to 2022 is illustrated in Figure 4. The data reveal that the monthly variation in SWC closely follows the southwest monsoonal rainfall pattern in India, with higher SWC observed during the monsoon season (June–September) and lower SWC during the pre-monsoon or summer season (March–May). Additionally, some parts of southern and north-eastern India exhibit higher SWC during the post-monsoon season (October–December)

due to rainfall received through the Northeast monsoon winds during this period. The northeastern parts of India also exhibited comparatively higher SWC during the pre-monsoon season, primarily due to rainfall received during Nor'westers (Kal Baisakhi).

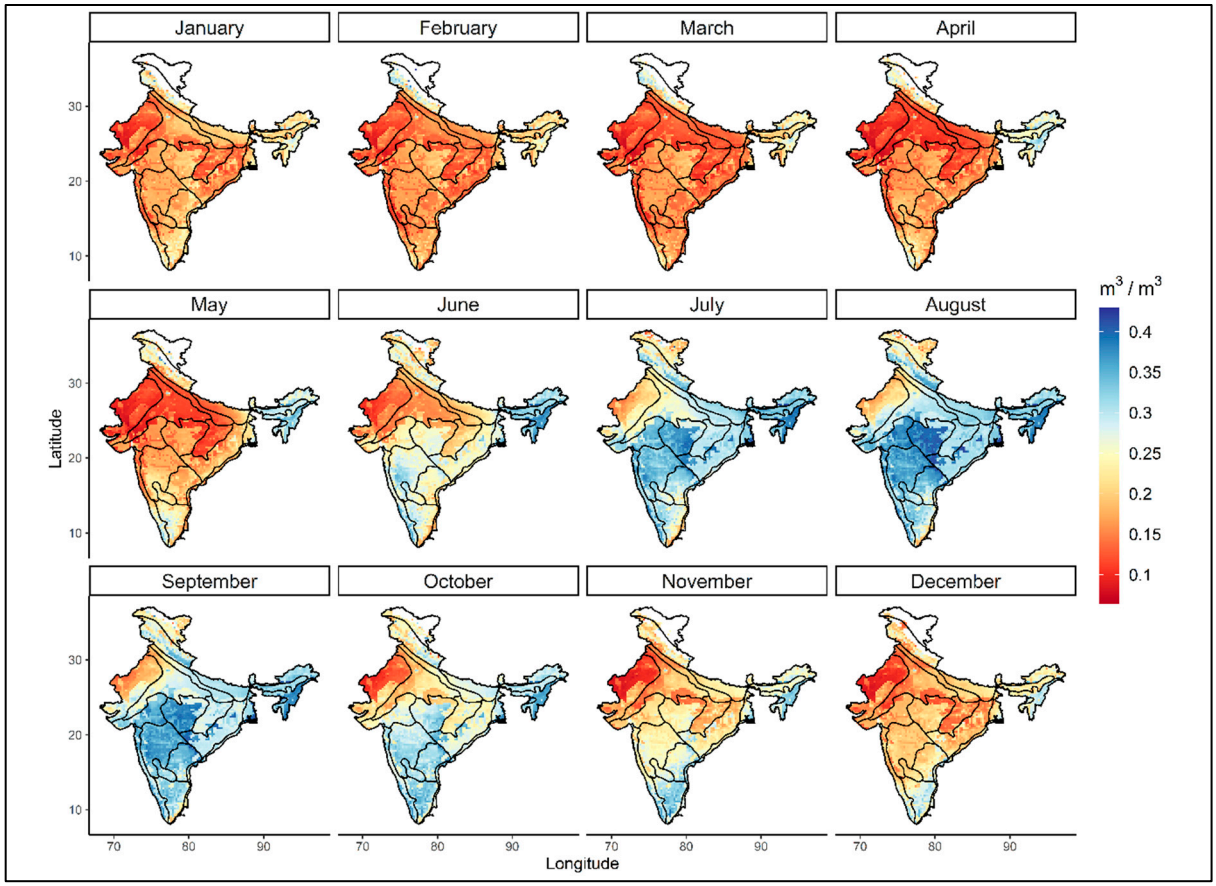

Figure 4. Monthly mean of ESA CCI near-surface SWC for the period of 44 years (1979 to 2022) under different AERs of mainland India.

3.2. Interannual Variation in the Near-Surface SWC

Figure 5 illustrates the interannual variations in near-surface SWC during the monsoon season (June–September) across different AERs and mainland India from 1979 to 2022. The analysis reveals notable fluctuations in monsoonal SWC over the study period. For mainland India, several years exhibited markedly lower monsoonal near-surface SWC compared with the long-term average. These years include 1979 (0.279 m^3 m^{-3}), 1982 (0.277 m^3 m^{-3}), 1987 (0.263 m^3 m^{-3}), 1992 (0.274 m^3 m^{-3}), 1993 (0.278 m^3 m^{-3}), 2002 (0.271 m^3 m^{-3}), 2009 (0.269 m^3 m^{-3}), 2012 (0.279 m^3 m^{-3}), 2014 (0.272 m^3 m^{-3}), and 2015 (0.275 m^3 m^{-3}). This pattern of lower SWC values in these specific years was generally consistent across most AERs, suggesting widespread climatic influences affecting soil moisture at the national scale. Spatial variability in SWC was evident among the AERs with AER-2 consistently displaying the lowest SWC values across most years, while AER-17 exhibited the highest SWC values. This spatial pattern persisted throughout the study period, indicating stable regional differences in soil moisture regimes, likely influenced by local climate, topography, and soil characteristics.

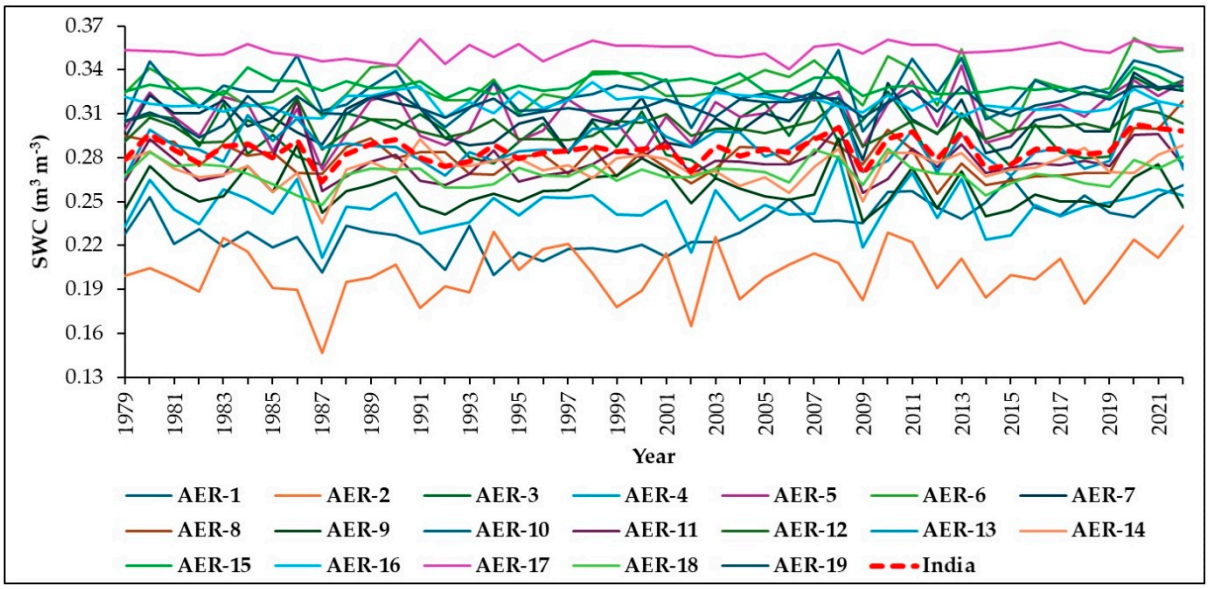

Figure 5. Interannual variations in the mean SWC of monsoon season (June–September) across different AERs and mainland India from 1979 to 2022 (44 years).

3.3. Spatiotemporal Trends in Near-Surface SWC

Figure 6 illustrates the spatial patterns of Sen's slope, depicting the magnitude of the temporal trend for each month. It includes spatial patterns and the percentage area of significantly increasing or decreasing trends ($p < 0.1$), as well as insignificant increasing or decreasing trends ($p > 0.1$) by the MK trend test in the near-surface SWC from 1979 to 2022. Figure 7 illustrates the same for the annual near-surface SWC for mainland India. Table 3 depicts the monthly and annual average Sen's slope value for each AER. Analysis of annual trends reveals that approximately 60% of mainland India exhibited an increasing temporal trend with varying statistical significance in near-surface SWC, with 17.96% of the area showing a significantly increasing trend ($p < 0.1$) and 7.6% demonstrating a significantly decreasing trend ($p < 0.1$). The average annual Sen's slope in mainland India was 0.9×10^{-4} m^3 m^{-3} $year^{-1}$. Among different AERs, the maximum percentage of the area under a significantly decreasing trend was found in the AER-16 (39%) followed by AER-15 (25%), and AER-17 (22.5%) with an average annual Sen's slope of -1.30×10^{-4}, -0.8×10^{-4}, and -0.6×10^{-4} m^3 m^{-3} $year^{-1}$, respectively. The maximum percentage of the area showing a significantly increasing trend was found in the AER-5 (40.9%) followed by AER-6 (33.4%) and AER-19 (29.5%) with an average Sen's slope of 2.6×10^{-4}, 1.8×10^{-4}, and 1.3×10^{-4} m^3 m^{-3} $year^{-1}$, respectively. AER-1 also showed 28.1% of the area with a significant increasing trend in annual SWC and a Sen's slope of 6.5×10^{-4} m^3/m^3 $year^{-1}$, although its data are not reliable due to missing data for many months.

Table 3. Monthly and annual average Sen's slope ($m^3\ m^{-3}\ year^{-1}$) of near-surface SWC from 1979 to 2022 for each AER of mainland India.

AER No.	January	February	March	April	May	June	July	August	September	October	November	December	Annual
AER-1	-	-	-3.14×10^{-3}	-1.19×10^{-2}	-8.47×10^{-3}	1.17×10^{-3}	1.14×10^{-3}	1.99×10^{-3}	-9.70×10^{-4}	-3.24×10^{-3}	-3.04×10^{-3}	1.61×10^{-3}	6.50×10^{-4}
AER-2	3.10×10^{-4}	-8.00×10^{-5}	-3.00×10^{-5}	1.00×10^{-5}	5.00×10^{-5}	3.80×10^{-4}	1.90×10^{-4}	3.00×10^{-5}	6.70×10^{-4}	2.30×10^{-4}	2.10×10^{-4}	2.80×10^{-4}	9.00×10^{-5}
AER-3	-1.00×10^{-5}	8.00×10^{-5}	2.00×10^{-5}	-1.00×10^{-4}	3.00×10^{-4}	1.00×10^{-4}	1.10×10^{-4}	1.10×10^{-4}	3.70×10^{-4}	7.40×10^{-4}	3.70×10^{-4}	6.00×10^{-4}	2.00×10^{-5}
AER-4	2.30×10^{-4}	-9.00×10^{-5}	-1.00×10^{-5}	0.00×10^{0}	1.20×10^{-4}	1.00×10^{-4}	2.10×10^{-4}	-1.60×10^{-4}	2.00×10^{-4}	-2.00×10^{-5}	3.30×10^{-4}	3.90×10^{-4}	5.00×10^{-5}
AER-5	2.00×10^{-4}	1.70×10^{-4}	7.00×10^{-5}	2.00×10^{-5}	2.00×10^{-5}	3.40×10^{-4}	5.80×10^{-4}	1.20×10^{-4}	8.40×10^{-4}	6.50×10^{-4}	6.00×10^{-4}	5.40×10^{-4}	2.60×10^{-4}
AER-6	1.70×10^{-4}	1.40×10^{-4}	8.00×10^{-5}	0.00×10^{0}	5.00×10^{-5}	5.30×10^{-4}	4.90×10^{-4}	3.00×10^{-4}	4.80×10^{-4}	8.30×10^{-4}	4.60×10^{-4}	4.90×10^{-4}	1.80×10^{-4}
AER-7	1.80×10^{-4}	7.00×10^{-5}	-6.00×10^{-5}	-1.40×10^{-4}	-1.90×10^{-4}	2.60×10^{-4}	1.00×10^{-4}	-6.00×10^{-5}	2.60×10^{-4}	3.40×10^{-4}	1.10×10^{-4}	3.90×10^{-4}	-6.00×10^{-5}
AER-8	1.70×10^{-4}	7.00×10^{-5}	7.00×10^{-5}	-3.00×10^{-5}	4.30×10^{-4}	-1.70×10^{-4}	-7.00×10^{-5}	1.50×10^{-4}	2.80×10^{-4}	5.70×10^{-4}	4.60×10^{-4}	8.20×10^{-4}	5.00×10^{-5}
AER-9	3.30×10^{-4}	-1.30×10^{-4}	-1.10×10^{-4}	-1.10×10^{-4}	1.30×10^{-4}	-1.90×10^{-4}	1.20×10^{-4}	-2.60×10^{-4}	-1.30×10^{-4}	1.00×10^{-4}	2.80×10^{-4}	4.60×10^{-4}	1.00×10^{-5}
AER-10	1.10×10^{-4}	7.00×10^{-5}	1.40×10^{-4}	0.00×10^{0}	2.00×10^{-5}	3.00×10^{-4}	2.20×10^{-4}	-4.00×10^{-5}	2.40×10^{-4}	3.00×10^{-4}	5.50×10^{-4}	4.30×10^{-4}	1.10×10^{-4}
AER-11	1.90×10^{-4}	2.00×10^{-5}	9.00×10^{-5}	-1.20×10^{-4}	1.70×10^{-4}	2.30×10^{-4}	2.70×10^{-4}	-2.00×10^{-5}	5.00×10^{-5}	3.90×10^{-4}	3.30×10^{-4}	3.30×10^{-4}	9.00×10^{-5}
AER-12	9.00×10^{-5}	-7.00×10^{-5}	-1.00×10^{-4}	-1.30×10^{-4}	7.00×10^{-5}	-4.00×10^{-5}	2.20×10^{-4}	1.80×10^{-4}	2.00×10^{-4}	3.30×10^{-4}	1.00×10^{-4}	2.40×10^{-4}	3.00×10^{-5}
AER-13	2.40×10^{-4}	-1.40×10^{-4}	-7.00×10^{-5}	-2.00×10^{-5}	2.00×10^{-4}	-2.00×10^{-5}	2.40×10^{-4}	-6.00×10^{-5}	-1.90×10^{-4}	1.20×10^{-4}	4.50×10^{-4}	3.10×10^{-4}	2.00×10^{-5}
AER-14	-1.23×10^{-3}	-2.00×10^{-4}	-8.40×10^{-4}	-1.42×10^{-3}	-5.30×10^{-4}	-1.30×10^{-4}	-2.00×10^{-5}	2.40×10^{-4}	4.90×10^{-4}	-3.70×10^{-4}	-8.10×10^{-4}	4.60×10^{-4}	7.00×10^{-5}
AER-15	6.00×10^{-5}	2.40×10^{-4}	-2.40×10^{-4}	-1.60×10^{-4}	-7.00×10^{-5}	-1.60×10^{-4}	5.00×10^{-5}	3.00×10^{-5}	-5.00×10^{-5}	-4.00×10^{-5}	-6.00×10^{-4}	2.00×10^{-5}	-8.00×10^{-5}
AER-16	-1.09×10^{-3}	-4.70×10^{-4}	-1.06×10^{-3}	-5.10×10^{-4}	1.20×10^{-4}	1.90×10^{-4}	5.00×10^{-5}	-2.00×10^{-5}	0.00×10^{0}	1.30×10^{-4}	-2.60×10^{-4}	-7.10×10^{-4}	-1.30×10^{-4}
AER-17	1.10×10^{-4}	-9.00×10^{-5}	-6.00×10^{-4}	-2.60×10^{-4}	2.00×10^{-4}	1.30×10^{-4}	1.40×10^{-4}	8.00×10^{-5}	5.00×10^{-5}	2.10×10^{-4}	2.20×10^{-4}	-3.00×10^{-5}	-6.00×10^{-5}
AER-18	9.30×10^{-4}	3.90×10^{-4}	1.60×10^{-4}	-1.20×10^{-4}	-3.00×10^{-5}	-6.80×10^{-4}	-9.00×10^{-5}	4.60×10^{-4}	2.70×10^{-4}	-1.00×10^{-5}	7.90×10^{-4}	1.95×10^{-3}	2.00×10^{-5}
AER-19	4.10×10^{-4}	1.40×10^{-4}	2.60×10^{-4}	1.20×10^{-4}	3.50×10^{-4}	4.70×10^{-4}	4.00×10^{-4}	2.90×10^{-4}	4.20×10^{-4}	3.60×10^{-4}	3.10×10^{-4}	6.80×10^{-4}	1.30×10^{-4}
India	1.30×10^{-4}	3.00×10^{-6}	-7.00×10^{-5}	-1.40×10^{-4}	4.00×10^{-5}	1.70×10^{-4}	2.40×10^{-4}	1.20×10^{-4}	2.60×10^{-4}	2.50×10^{-4}	2.50×10^{-4}	4.00×10^{-4}	0.9×10^{-4}

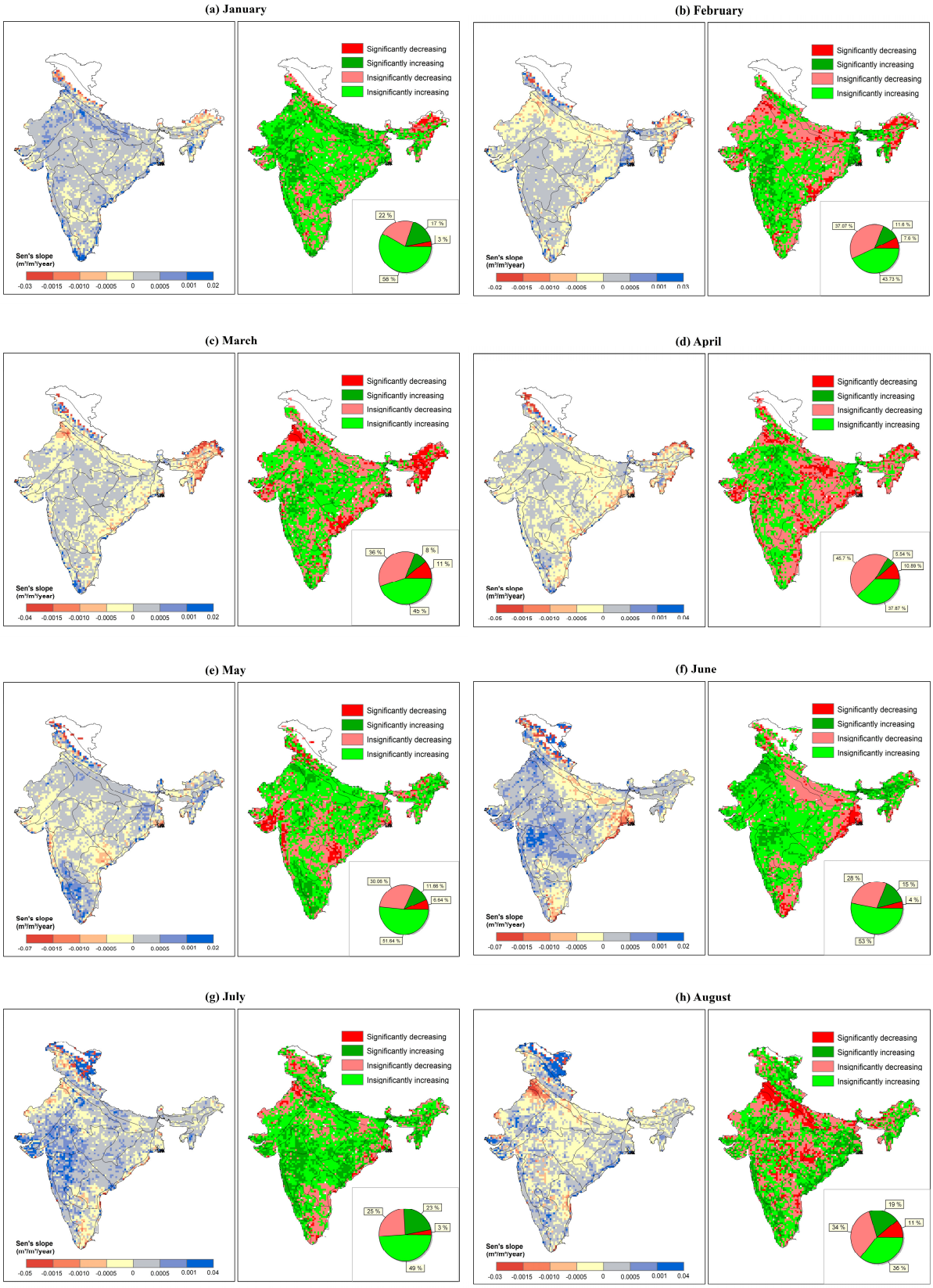

Figure 6. *Cont.*

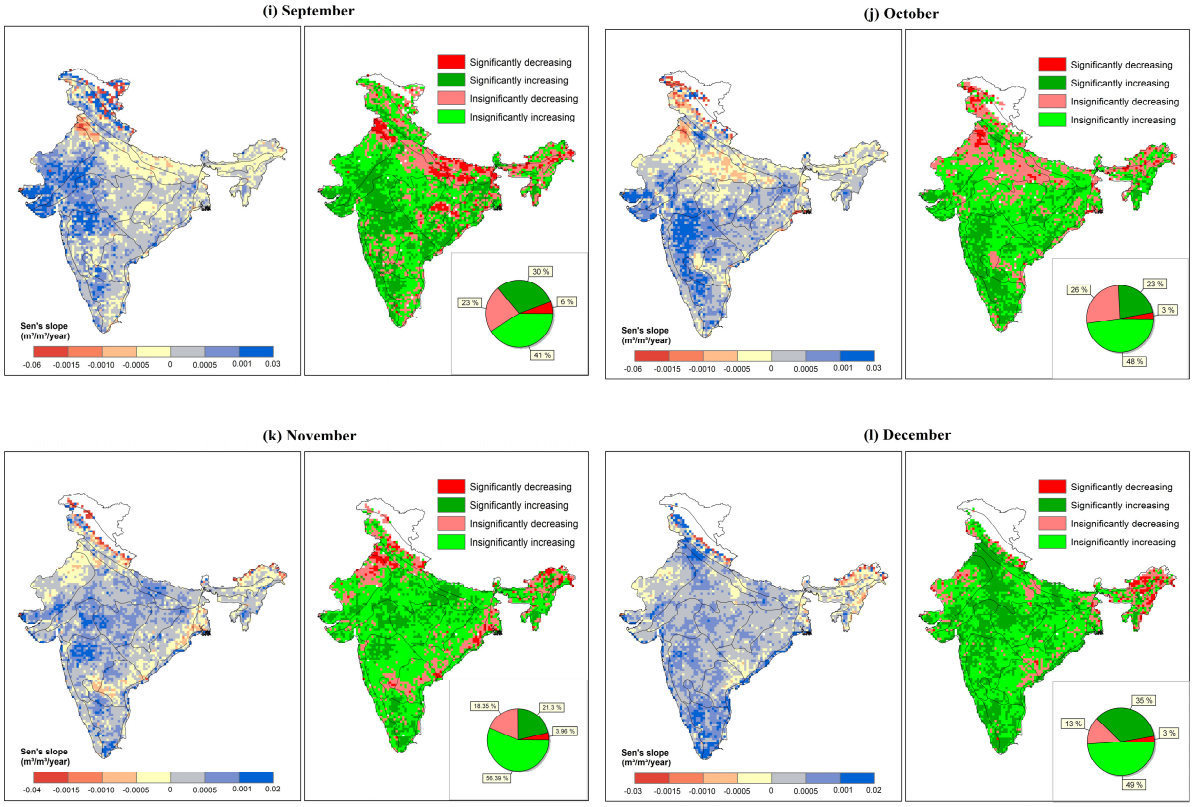

Figure 6. Spatial patterns of the magnitude of temporal trend (indicated by Sen's slope (m^3 m^{-3} $year^{-1}$)) and direction of the significant ($p < 0.1$) and insignificant ($p > 0.1$) temporal trend (indicated by MK trend test) in the near-surface SWC for each month from 1979 to 2022.

Monthly trend analysis revealed significant variations in near-surface SWC trends across different seasons. December showed the highest percentage of areas with significantly increasing trends (35%), followed by September (30%), October (23%), July (23%), and November (21.3%). The average Sen's slopes for these months ranged from 2.4×10^{-4} to 4×10^{-4} m^3 m^{-3} $year^{-1}$. In contrast, March and April exhibited the largest areas with significantly decreasing trends (11% each), with average Sen's slopes of -7.00×10^{-5} and -1.40×10^{-4} m^3 m^{-3} $year^{-1}$, respectively. Notably, August displayed both significantly increasing (19%) and decreasing (11%) trends across different regions, with an average Sen's slope of 1.2×10^{-4} m^3 m^{-3} $year^{-1}$, highlighting the spatial variability in SWC trends even within a single month.

Substantial variability was observed in the trend patterns of near-surface soil water content (SWC) across different AERs and months in mainland India. This variability highlights the complex spatiotemporal patterns likely influenced by regional climate variability, land use changes, and local hydrological conditions. In January, AER-16 showed the maximum percentage of areas with a significantly decreasing trend (39.8%) with an average Sen's slope of -1.09×10^{-3} m^3 m^{-3} $year^{-1}$. Conversely, several AERs showed significantly increasing trends, including AER-19 (31.4%), AER-5 (30.8%), AER-13 (29.5%), AER-2 (29%), AER-9 (29%), and AER-18 (28.4%). The average Sen's slopes for these increasing trends ranged from 2.0×10^{-4} to 9.3×10^{-4} m^3 m^{-3} $year^{-1}$. February presented a different pattern, with AER-4 showing the maximum area under a significantly decreasing trend (39.8%) and an average Sen's slope of -0.9×10^{-4} m^3 m^{-3} $year^{-1}$. The areas with significantly increasing trends were found in AER-10 (31.4%), AER-15 (30.8%), AER-6 (29.5%), and AER-8 (29%), with average Sen's slopes ranging from 7.00×10^{-5} to 2.40×10^{-4} m^3 m^{-3} $year^{-1}$.

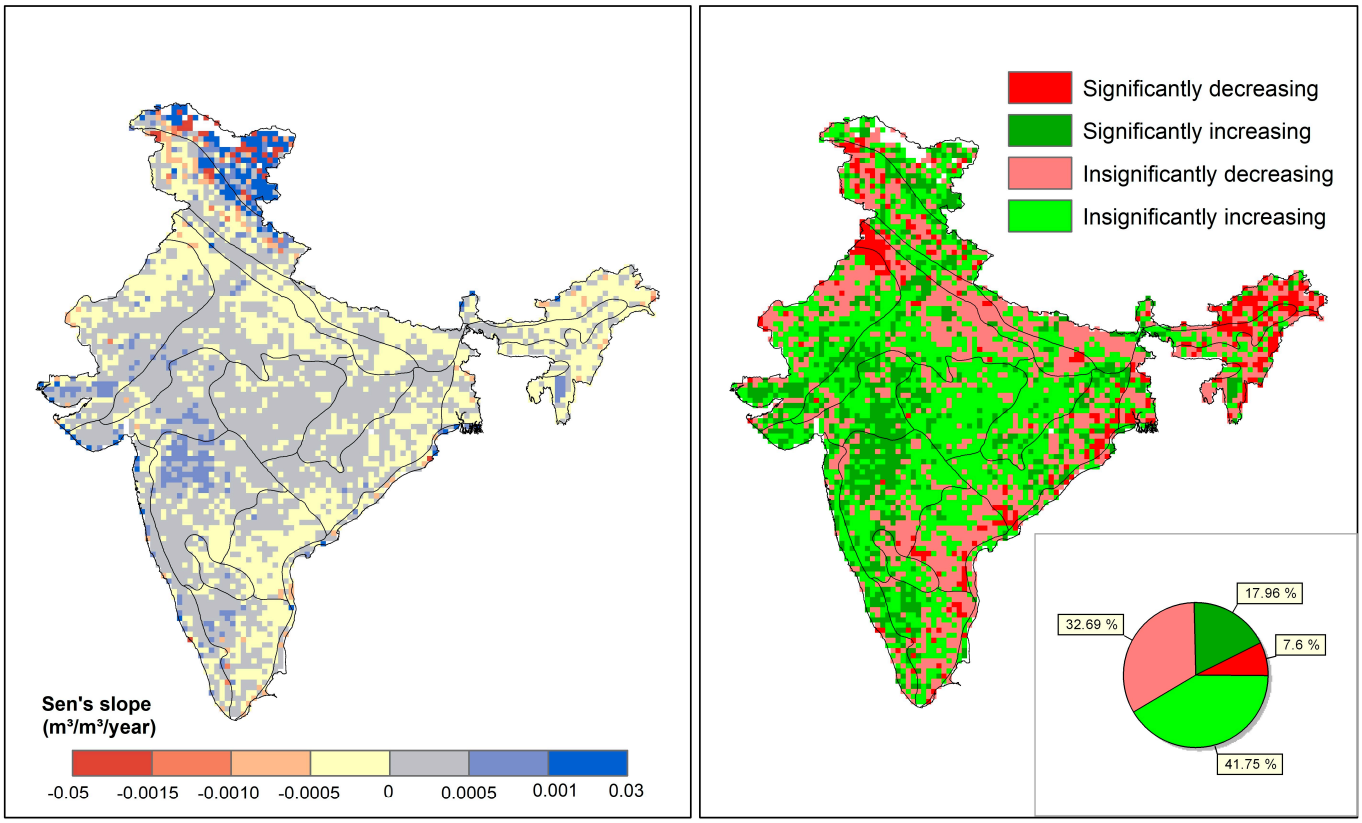

Figure 7. Spatial patterns of the magnitude of temporal trend (indicated by Sen's slope (m^3 m^{-3} $year^{-1}$)) and direction of the significant ($p < 0.1$) and insignificant ($p > 0.1$) temporal trend (indicated by MK trend test) in the annual near-surface SWC from 1979 to 2022.

March exhibited strong decreasing trends in several AERs, with AER-17 (50%), AER-16 (49.2%), and AER-15 (33.5%) showing the largest areas under significantly decreasing trends. The average Sen's slopes for these regions were -6.00×10^{-4}, -1.06×10^{-3}, and -2.40×10^{-4} m^3 m^{-3} $year^{-1}$, respectively. AER-19 showed the maximum area with a significantly increasing trend (25%) and an average Sen's slope of 2.60×10^{-4} m^3 m^{-3} $year^{-1}$. In April, AER-16 continued to show a significantly decreasing trend over 30.8% of its area, with an average Sen's slope of -5.10×10^{-4} m^3 m^{-3} $year^{-1}$. Notably, no AER exhibited more than 20% area under a significantly increasing trend during this month. May saw a shift in trends, with no AER showing more than 20% area with significantly decreasing trends. However, AER-8 displayed a significantly increasing trend over 39.1% of its area, with an average Sen's slope of 4.30×10^{-4} m^3 m^{-3} $year^{-1}$.

June presented mixed trends across different AERs. AER-18 showed the maximum area with a significantly decreasing trend (27.3%) and an average Sen's slope of -6.80×10^{-4} m^3 m^{-3} $year^{-1}$. AER-19 exhibited the largest area with a significantly increasing trend (33.5%) and an average Sen's slope of 4.70×10^{-4} m^3 m^{-3} $year^{-1}$. Interestingly, AER-15 displayed both increasing and decreasing trends, with 31.1% area showing a significantly increasing trend and 24% area showing a significantly decreasing trend with an average Sen's slope of -1.60×10^{-4} m^3 m^{-3} $year^{-1}$. July marked a shift toward predominantly increasing trends. No AER showed more than 20% area with significantly decreasing trends, while significantly increasing trends were observed in AER-19 (52.9%), AER-6 (45.9%), and AER-5 (43%). The average Sen's slopes for these regions ranged from 4.00×10^{-4} to 5.80×10^{-4} m^3 m^{-3} $year^{-1}$. August displayed a mix of increasing and decreasing trends. AER-9 (44.3%) showed maximum area with a significantly decreasing trend followed by AER-4 (25.7%) with an average Sen's slope of 2.60×10^{-4} and -1.60×10^{-4} m^3 m^{-3} $year^{-1}$, respectively, while the maximum area with a significantly in-

creasing trend was found in the AER-19 (50.6%) followed by AER-12 (39%) and AER-18 (38.6%) with an average Sen's slope of 2.90×10^{-4}, 1.80×10^{-4}, and 4.60×10^{-4} m^3 m^{-3} $year^{-1}$, respectively. September continued to show variability, with AER-13 (34.8%) and AER-9 (23.4%) displaying the largest areas of significantly decreasing trends with an average Sen's slope of -1.90×10^{-4} and -1.30×10^{-4} m^3 m^{-3} $year^{-1}$, respectively. However, several AERs showed substantial areas with significantly increasing trends, including AER-5 (65.6%), AER-19 (53.2%), AER-6 (49.1%), and AER-12 (45.4%) with an average Sen's slope ranging from 2.00×10^{-4} to 8.40×10^{-4} m^3 m^{-3} $year^{-1}$.

October marked a shift toward predominantly increasing trends, with no AER showing more than 20% area under significantly decreasing trends, while the maximum area under significantly increasing trend was found in AER-8 (59.7%) followed by AER-3 (53%) and AER-6 (48.5%) with an average Sen's slope of 5.70×10^{-4}, 7.40×10^{-4}, and 8.30×10^{-4} m^3 m^{-3} $year^{-1}$, respectively. In November, AER-16 showed the maximum area with a significantly decreasing trend (24.2%) and an average Sen's slope of -2.60×10^{-4} m^3 m^{-3} $year^{-1}$. Several AERs exhibited significantly increasing trends, including AER-10 (39.2%), AER-8 (39%), AER-5 (37.6%), and AER-13 (32.5%) with an average Sen's slope of 5.50×10^{-4}, 4.6×10^{-4}, 6.00×10^{-4}, and 4.50×10^{-4} m^3 m^{-3} $year^{-1}$, respectively. December displayed a pattern similar to November, with AER-16 showing the largest area of a significantly decreasing trend (27.4%) and an average Sen's slope of -7.10×10^{-4} m^3 m^{-3} $year^{-1}$. However, numerous AERs exhibited substantial areas with significantly increasing trends, including AER-5 (57.4%), AER-18 (55.7%), AER-8 (54.4%), AER-19 (52.6%), AER-4 (49.3%), AER-10 (49.2%), and AER-9 (43.8%). The average Sen's slopes for these increasing trends ranged from 0.39 to 1.95×10^{-3} m^3 m^{-3} $year^{-1}$.

3.4. Temporal Association of Near-Surface SWC with Environmental Variables

The temporal association between near-surface SWC and environmental variables, including rainfall, temperature, actual evapotranspiration, and NDVI, was investigated using Spearman's rank correlation coefficient (ρ). The spatial pattern of significant ($p < 0.1$) Spearman's correlation coefficient (ρ) between the time-series datasets of near-surface SWC with rainfall, temperature, actual evapotranspiration, and NDVI is depicted in Figure 8. The average Spearman's correlation coefficient for each AER is presented in Table 4. The Spearman's correlation coefficient of near-surface SWC with rainfall ranged from 0.09 (AER-1) to 0.80 (AER-6) with an average value of 0.70 for mainland India as a whole. Most AERs exhibited a strong correlation ($\rho > 0.6$) with rainfall, indicating a close relationship between precipitation events and near-surface SWC. In contrast to rainfall, near-surface SWC showed a negative or weak correlation with temperature, ranging from −0.30 (AER-8) to 0.80 (AER-17), with an average value of 0.12 for mainland India. This suggests minimal or even an inverse relationship between temperature and SWC across mainland India. Interestingly, AER-15 ($\rho = 0.63$), AER-16 ($\rho = 0.73$), and AER-17 ($\rho = 0.80$), which also exhibited declining temporal trends in near-surface SWC, showed highly positive correlations with temperature. The correlation of near-surface SWC with actual evapotranspiration varied from 0.36 (AER-1) to 0.88 (AER-6 and AER-11), averaging 0.74 for mainland India. In most AERs, the correlation with actual evapotranspiration was above 0.60, indicating a strong association between actual evapotranspiration and SWC. Similarly, the correlation of near-surface SWC with NDVI ranged from -0.06 (AER-1) to 0.85 (AER-17), with an average value of 0.65. This trend mirrored the relationship observed with actual evapotranspiration where most AERs exhibited a positive correlation greater than 0.6, suggesting a close link between vegetation health (as indicated by NDVI) and SWC.

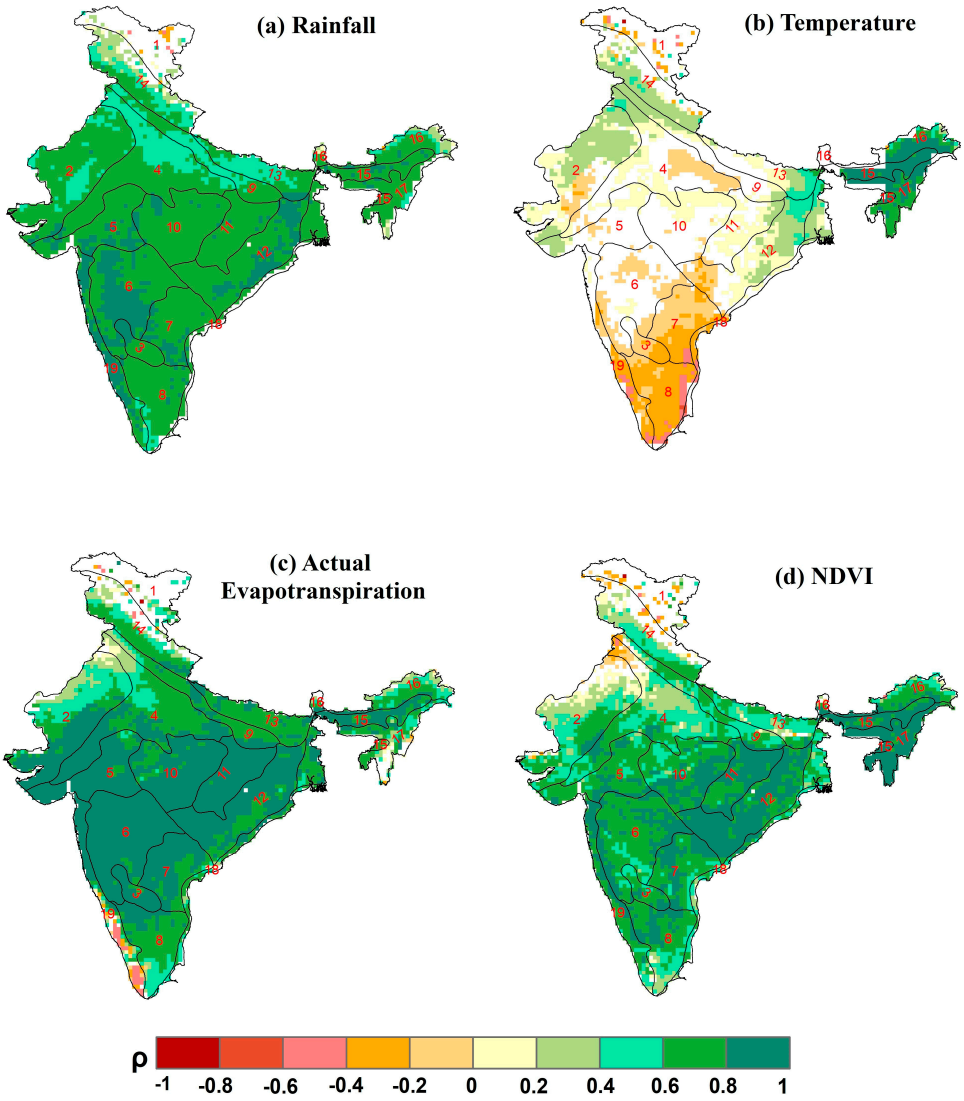

Figure 8. Spatial pattern of the significant Spearman's rank correlation coefficient (ρ) ($p < 0.1$) of near-surface SWC with (**a**) rainfall, (**b**) temperature, (**c**) actual evapotranspiration, and (**d**) NDVI.

Table 4. Average Spearman's correlation coefficient (ρ) of the near-surface SWC with environmental variables for each AER of mainland India.

AER No.	Rainfall	Temperature	Actual Evapotranspiration	NDVI
AER-1	0.09	−0.21	0.36	−0.06
AER-2	0.67	0.19	0.65	0.43
AER-3	0.79	−0.19	0.83	0.72
AER-4	0.65	0.07	0.72	0.49
AER-5	0.78	0.11	0.87	0.71
AER-6	0.80	−0.10	0.88	0.75
AER-7	0.77	−0.21	0.81	0.76
AER-8	0.72	−0.30	0.70	0.66
AER-9	0.62	0.21	0.73	0.56
AER-10	0.77	0.09	0.86	0.73
AER-11	0.75	0.13	0.88	0.80
AER-12	0.78	0.17	0.83	0.83
AER-13	0.63	0.29	0.76	0.55
AER-14	0.47	0.26	0.54	0.37
AER-15	0.74	0.63	0.79	0.72
AER-16	0.59	0.73	0.56	0.65

Table 4. *Cont.*

AER No.	Rainfall	Temperature	Actual Evapotranspiration	NDVI
AER-17	0.68	0.80	0.55	0.85
AER-18	0.75	−0.15	0.67	0.56
AER-19	0.78	−0.26	0.39	0.73
India	0.70	0.12	0.74	0.65

4. Discussion

This study examined the spatiotemporal variations and trends in near-surface SWC across different AERs in mainland India over a 44-year period (1979–2022) using ESA CCI SM data. The temporal relationships between SWC and climatic variables (rainfall, temperature) alongside response variables (actual evapotranspiration, NDVI) were also explored. The primary driver controlling near-surface SWC across different AERs is rainfall, as evidenced by its strong correlation ($\rho = 0.70$) with SWC, highlighting the crucial role of precipitation in determining soil moisture levels. The spatial heterogeneity in SWC across various AERs and the distinct monthly variations are closely tied to the seasonal patterns of monsoonal rainfall. The monthly mean near-surface SWC data from 1979 to 2022 reveal a clear alignment with the Southwest monsoonal rainfall pattern, with higher SWC during the monsoon season (June–September) and lower SWC during the pre-monsoon or summer season (March–May) [71]. Additionally, the post-monsoon season (October–December) sees elevated SWC levels in southern and northeastern regions due to rainfall from the Northeast monsoon [72], highlighting the dual influence of both monsoon systems on soil moisture dynamics. Apart from that, the higher SWC in northeast India during the pre-monsoon season was found primarily due to rainfall received from Nor'westers or Kal Baisakhi [73]. The spatial patterns of SWC variation across different months align well with the onset, progression, and withdrawal of the Southwest and Northeast monsoons, emphasizing the critical role of monsoonal rains in replenishing SWC across India (Figure 4). These findings are consistent with previous studies by Sathyanadh et al. [32], Zheng et al. [74], Varikoden and Revadekar [75], and Guntu and Agarwal [76], all of which highlight the significant impact of monsoonal rainfall on soil moisture dynamics.

The analysis of near-surface SWC across various AERs of mainland India underscores significant spatial variability, driven by distinct climatic conditions, soil types, and topographical features inherent to each region (Figure 3). The lowest average annual SWC values observed in AER-2 (0.15 $m^3\ m^{-3}$) and AER-4 (0.18 $m^3\ m^{-3}$) highlight the challenges posed by the hot arid and semi-arid environments of these regions. AER-2, encompassing the western plains of Kachchh and parts of the Kathiawar Peninsula, is characterized by extreme aridity, minimal annual rainfall (<40 cm), and high evaporation rates, leading to persistently low soil moisture levels. Similarly, AER-4, covering parts of Gujarat, northern plains, and the Central Highlands, experiences hot and dry summers with moderate rainfall (50–100 cm), contributing to lower soil moisture retention. Conversely, the highest average annual SWC values in AER-17 (0.30 $m^3\ m^{-3}$), AER-16 (0.28 $m^3\ m^{-3}$), and AER-15 (0.27 $m^3\ m^{-3}$) can be attributed to the favorable climatic conditions of these regions. AER-17, representing the warm per-humid regions of the northeastern hills, benefits from substantial annual rainfall (200–300 cm) and a long growing period (>270 days), resulting in consistently high soil moisture levels. Similarly, AER-16, located in the Eastern Himalayas, and AER-15, covering the Bengal Basin and Assam Plain, receive abundant rainfall and have extended growing seasons, enhancing SWC [51].

The coefficient of variation (CV) in near-surface SWC, ranging from 1.93% to 57.28% with an average of 28.90%, further illustrates the pronounced spatial variability across mainland India (Figure 2). Regions in the northwestern, western, eastern, and central parts of India exhibit high variability, with CVs exceeding 30%, indicating significant fluctuations in SWC. This variability can be linked to the diverse climatic and soil conditions, ranging from arid deserts to semi-arid plains. In contrast, northern, northeastern, and parts of southern India, with CVs below 20%, exhibit more stable soil moisture regimes, benefiting

from consistent rainfall patterns and favorable soil properties. The spatial pattern of CV variation in SWC aligns closely with the variability observed in rainfall CV across India, as noted by Praveen et al. [77]. The interannual variation in near-surface SWC reveals notable years, such as 1979, 1982, 1987, 1992, 1993, 2002, 2009, 2012, 2014, and 2015, marked by consistently lower SWC levels (Figure 5). These years coincide with periods of significant drought across many regions of India [78–80]. This alignment underscores the susceptibility of SWC to climatic anomalies and highlights the critical influence of drought events on soil moisture dynamics. This also highlights the applicability of ESA CCI near-surface SWC for drought monitoring and forecasting.

The analysis of near-surface SWC trends reveals significant spatial and temporal variability across different AERs and months in mainland India. Approximately 60% of the area shows an increasing trend in annual SWC, with varying levels of statistical significance (Figure 7). This finding closely aligns with Kumar et al. [81], who reported a significant increasing trend in annual rainfall across approximately half of India's subdivisions. This concurrence underscores the critical influence of rainfall patterns on SWC dynamics. Additionally, the increase in irrigated areas, as noted by Jain et al. [49], may also contribute to the rising annual SWC trends. The predominance of increasing SWC trends during certain months, particularly during the monsoon and post-monsoon seasons (Figure 6f–l), suggests potential changes in rainfall intensity and distribution, consistent with observations by Guhathakurta and Rajeevan [82] who reported increasing rainfall trends in most subdivisions during these seasons. Conversely, the decreasing SWC trends observed in some regions during the pre-monsoon months (Figure 6c,d) align with the decreasing rainfall trends reported by Guhathakurta and Rajeevan [82] for the same period.

The trends in near-surface SWC across AERs in mainland India reveal significant variability influenced by diverse environmental factors and human activities. AER-5 (hot semi-arid ecoregion with medium and deep black soils) and AER-6 (hot semi-arid ecoregion with shallow and medium black soils) displayed the highest percentage of areas with significant increasing trends throughout the year. These regions are characterized by black soils with good water-holding capacities, which could potentially contribute to the observed positive trends in SWC. AER-19 (Hot humid per-humid ecoregion with red, lateritic, and alluvium-derived soils) also showed an increasing trend in SWC. Singh et al. [83], and Guhathakurta and Rajeevan [82] also exhibited increasing rainfall trends in these areas. Conversely, AER-16 (warm per-humid ecoregion with brown and red hill soils) and AER-17 (warm per humid ecoregion with red and lateritic soils) showed the highest percentage of areas with significant decreasing trends, corresponding to reported declines in regional rainfall documented by Oza and Kishtawal [84], Patle and Libang [85], and Singh et al. [83]. These trends are attributed to climate change impacts affecting regional precipitation patterns, eventually affecting the SWC. Furthermore, AER-15, AER-16, and AER-17 show declining SWC trends potentially linked to soil degradation from shifting cultivation practices or land use changes converting forest areas to agricultural lands. These activities contribute to soil erosion and depletion of SWC, as noted by Jaiswal and Amin [86] and Marchang [87]. AER-1, classified as a cold arid ecoregion with shallow skeletal soils, showed a high percentage of increasing trends in annual SWC despite weaker correlations ($\rho = 0.09$) with rainfall. The rainfall trend is also decreasing in AER-1, but the increasing trend in SWC may be due to the melting of glaciers caused by global warming [88]. However, interpreting trends in this region requires caution due to data scarcity. The variation in SWC trends in each AER was found between different months (Figure 6). This could be attributed to regional variations in rainfall patterns, temperature changes, potential shifts in monsoon intensity, changes in land use practices, irrigation, topography, etc., which need further detailed investigation.

The analysis of near-surface SWC across AERs in mainland India reveals intricate relationships with climatic variables, highlighting significant spatial and temporal variability (Figure 8). Weak or negative correlations between SWC and temperature suggest that rising temperatures may exacerbate soil moisture depletion, particularly in regions

already experiencing declining SWC (Figure 8). This phenomenon suggests that high evapotranspiration rates under intense summer heat could contribute to rapid soil moisture loss, despite overall positive correlations between SWC and rainfall observed in most AERs (Figure 8). However, AERs like 15, 16, and 17, which exhibit declining SWC trends, paradoxically show positive correlations with temperature [89]. This anomaly underscores the multifaceted nature of climate impacts on SWC where rising temperatures coupled with declining rainfall may exacerbate moisture deficits.

A strong positive correlation (average $\rho = 0.74$) between SWC and actual evapotranspiration across AERs indicates that vegetation water use closely influences soil moisture dynamics (Figure 8). Regions with high evapotranspiration rates, such as AER-6 ($\rho = 0.88$), likely experience significant SWC depletion due to intense water transpiration by vegetation [90]. In contrast, AER-1 shows a weaker correlation ($\rho = 0.36$), attributed to sparse vegetation cover and limited evapotranspiration potential, highlighting how vegetation dynamics mediate SWC variations. The correlation between SWC and NDVI, a proxy for vegetation health, reinforces these findings (Figure 8). Higher NDVI indicates stronger links between vegetation water use and SWC, with denser vegetation in AERs exhibiting more pronounced correlations between SWC and NDVI. Conversely, regions with sparse vegetation, like AER-1, show negligible influence of vegetation on SWC.

Overall, these findings underscore the complex interplay of climate factors, vegetation dynamics, and local management practices in shaping SWC variability across AERs in India. Effective water management strategies must consider these dynamics to enhance soil moisture retention, optimize irrigation efficiency, and sustainably manage water resources amidst changing climatic conditions. Acknowledging data limitations and the influence of local factors beyond AER classifications is crucial for accurately interpreting SWC trends and implementing targeted water conservation measures.

5. Conclusions

This study investigated the spatiotemporal variations and trends in near-surface SWC across diverse AERs of mainland India over a 44-year period (1979–2022) using ESA CCI data surface soil moisture data. Rainfall emerged as the primary driver of SWC variations across AERs, with a strong positive correlation ($\rho = 0.70$). Spatial patterns of SWC variation closely matched the seasonality of monsoonal rainfall, highlighting their critical role in replenishing soil moisture. The spatial variability in SWC across various AERs is significant, with distinct differences observed between regions. Interannual variation in SWC reveals notable years with consistently lower SWC levels, such as 1979, 1982, 1987, 1992, 1993, 2002, 2009, 2012, 2014, and 2015, coinciding with significant drought periods across many regions of India exhibiting the potential of ESA CCI near-surface SWC data for drought monitoring and early warning systems.

Approximately 60% of mainland India exhibited an increasing trend in annual SWC, with varying levels of statistical significance. Notably, 17.96% of the area showed a significantly increasing trend ($p < 0.1$), while 7.6% demonstrated a significantly decreasing trend with an average annual Sen's slope of 0.9×10^{-4} m^3 m^{-3} $year^{-1}$. The areas with the highest significant decreases were AER-16 (39%), AER-15 (25%), and AER-17 (22.5%), highlighting the need for targeted water conservation measures in these areas. In contrast, AER-5, AER-6, and AER-19 had the largest significant increases, suggesting the importance of enhanced drainage facilities in these regions.

December showed the highest percentage of area with significantly increasing trends (35%), followed by September (30%), October (23%), July (23%), and November (21%). March and April exhibited the largest areas with significantly decreasing trends (11% each). August displayed both significantly increasing (19%) and decreasing (11%) trends, highlighting the spatial variability in SWC trends, even within a single month. These monthly trends have important implications for targeted water resource management.

SWC trends correlated closely with rainfall trends, indicating climate change impacts. Human factors like irrigation and land use change also contribute to SWC trends. The cor-

relation analysis highlights the complexity of factors influencing SWC variability. Weak or negative correlations between SWC and temperature suggest that rising temperatures may adversely affect soil moisture. AER-15 ($\rho = 0.63$), AER-16 ($\rho = 0.73$), and AER-17 ($\rho = 0.80$) showed highly positive correlations with temperature, indicating complex climate impacts on SWC. A strong positive correlation between SWC and actual evapotranspiration (average $\rho = 0.74$) and NDVI (average $\rho = 0.65$) highlighted the close association between plant water use and available soil moisture. Regions with higher vegetation density displayed a stronger link between SWC and vegetation water use.

This study underscores the intricate relationships between climatic factors and SWC in mainland India, providing valuable insights for sustainable water resource management and agricultural planning. Further research is needed to explore specific mechanisms driving the observed trends in SWC, involving climatic teleconnections, land use/land cover change data, and hydrological modeling approaches. This deeper understanding is crucial for sustainable water resource management in the context of a changing climate.

Author Contributions: Conceptualization, A.R., N.K.S. and N.K.L.; data curation, J.K. and D.K.; formal analysis, A.R. and N.K.S.; funding acquisition, A.S.; investigation, A.R., B.J. and R.M.; methodology, A.R., N.K.S., N.K.L. and M.M.; project administration, R.S.C. and N.K.L.; resources, S.J., R.S.C. and N.K.L.; supervision, N.K.L.; validation, A.R., R.M. and N.K.S., visualization, A.R.; writing—original draft, A.R., N.K.S. and R.M.; writing—review and editing, P.S., N.K.L., N.K. and A.S. All authors have read and agreed to the published version of the manuscript.

Funding: This research received no external funding.

Data Availability Statement: The datasets utilized in this study are publicly accessible. The ESA CCI soil moisture data can be retrieved from https://www.esa-soilmoisture-cci.org/ (accessed on 15 June 2024). Gridded IMD rainfall data are available for download at https://www.imdpune.gov.in/cmpg/Griddata/Rainfall_25_NetCDF.html (accessed on 15 June 2024), while gridded maximum and minimum temperature data can be found at https://www.imdpune.gov.in/cmpg/Griddata/Max_1_Bin.html (accessed on 15 June 2024) and https://www.imdpune.gov.in/cmpg/Griddata/Min_1_Bin.html (accessed on 15 June 2024), respectively. NDVI data were sourced from https://zenodo.org/doi/10.5281/zenodo.4305974 (accessed on 15 June 2024) and https://search.earthdata.nasa.gov/ (accessed on 15 June 2024). Gridwise trend and correlation data that support the findings of this study are available upon request from the corresponding author.

Acknowledgments: The authors extend their gratitude to the Director of the Indian Institute of Soil Science, Bhopal, for the logistic support provided in conducting this research. We also acknowledge the European Space Agency for the provision of the near-surface soil water content data, the India Meteorological Department for the rainfall and temperature data, NASA for the actual evapotranspiration data from MODIS, and Zenodo for long-term NDVI data. Their contributions were essential for the successful completion of this study.

Conflicts of Interest: The authors declare no conflicts of interest.

References

1. Luo, X.; Li, S.; Yang, W.; Liu, L.; Shi, Y.; Lai, Y.; Yu, P.; Yang, Z.; Luo, K.; Zhou, T.; et al. Spatio-temporal changes in global root zone soil moisture from 1981 to 2017. *J. Hydrol.* **2023**, *626*, 130297. [CrossRef]
2. IPCC. Climate Change 2014: Synthesis Report. In *Contribution of Working Groups I, II and III to the Fifth Assessment Report of the Intergovernmental Panel on Climate Change*; Core Writing Team, Pachauri, R.K., Meyer, L.A., Eds.; IPCC: Geneva, Switzerland, 2014; Volume 151.
3. Datta, P.; Das, S. Analysis of long-term precipitation changes in West Bengal, India: An approach to detect monotonic trends influenced by autocorrelations. *Dyn. Atmos. Oceans.* **2019**, *88*, 101–118. [CrossRef]
4. Sinha, N.K.; Mohanty, M.; Somasundaram, J.; Chaudhary, R.S.; Patra, H.; Hati, K.M.; Singh, R.P.; Thakur, J.K.; Kumar, J.; Kumar, D.; et al. Maize productivity analysis in response to climate change under different nitrogen management strategies. *J. Agrometeorol.* **2021**, *23*, 279–285. [CrossRef]
5. Srivastava, A.; Kumari, N.; Maza, M. Hydrological response to agricultural land use heterogeneity using variable infiltration capacity model. *Water Resour. Manag.* **2020**, *34*, 3779–3794. [CrossRef]
6. Shah, H.L.; Mishra, V. Hydrologic Changes in Indian Sub-continental River Basins (1901–2012). *J. Hydrometeorol.* **2016**, *17*, 2667–2687. [CrossRef]

7. Mallick, T.; Pandidurai, D.; Sharma, D.; Sharma, A.; Panda, S.K. A comparative assessment of meteorological drought characteristics in agro-climatic zones of Rajasthan (arid) and Tamil Nadu (humid), India. *Nat. Hazards* **2024**, *120*, 4181–4203. [CrossRef]
8. Pandey, K.B.; Khare, D. Identification of Trend in Long Term Precipitation and Reference Evapotranspiration over Narmada River Basin (India). *Glob. Planet Chang.* **2018**, *161*, 172–182. [CrossRef]
9. Goswami, B.N.; Venugopal, V.; Sengupta, D.; Madhusoodanan, M.S.; Xavier, P.K. Increasing trend of extreme rain events over India in a warming environment. *Science* **2006**, *314*, 1442–1445. [CrossRef]
10. Ramesh, K.V.; Goswami, P. The shrinking Indian summer monsoon. In *Research Report RR CM 0709*; CSIR Centre for Mathematical Modelling and Computer Simulation: Bangalore, India, 2007.
11. Kothawale, D.R.; Revadekar, J.V.; Kumar, K.R. Recent trends in pre-monsoon daily temperature extremes over India. *J. Earth Syst. Sci.* **2010**, *119*, 51–65. [CrossRef]
12. Arora, M.; Goel, N.K.; Singh, P. Evaluation of temperature trends over India. *Hydrol. Sci. J.* **2005**, *50*, 81–93. [CrossRef]
13. Sen, R.S.; Balling, R.C. Trends in extreme daily precipitation indices in India. *Int. J. Climatol.* **2004**, *24*, 457–466. [CrossRef]
14. Andrighetti, M.; Zardi, D.; Franceschi, M. History and analysis of the temperature series of Verona (1769–2006). *Meteorol. Atmos. Phys.* **2009**, *103*, 267–277. [CrossRef]
15. Pal, I.; Al-Tabbaa, A. Regional changes in extreme monsoon rainfall deferent and excess in India. *Dyn. Atmos. Oceans* **2010**, *49*, 206–214. [CrossRef]
16. Pal, I.; Al-Tabbaa, A. Long-term changes and variability of monthly extreme temperatures in India. *Theor. Appl. Climatol.* **2010**, *100*, 45–56. [CrossRef]
17. Gosain, A.K.; Rao, S.; Basuray, D. Climate change impact assessment on hydrology of Indian river basins. *Curr. Sci.* **2006**, *90*, 346–353.
18. Kumari, N.; Srivastava, A.; Dumka, U.C. A long-term spatiotemporal analysis of vegetation greenness over the Himalayan Region using Google Earth Engine. *Climate* **2021**, *9*, 109. [CrossRef]
19. Taylor, K.E.; Stouffer, R.J.; Meehl, G.A. An overview of CMIP5 and the experiment design. *Bull. Am. Meteorol. Society* **2012**, *93*, 485–498. [CrossRef]
20. Mohanty, M.; Sinha, N.K.; Somasundaram, J.; McDermid, S.S.; Patra, A.K.; Singh, M.; Dwivedi, A.K.; Reddy, K.S.; Rao, C.S.; Prabhakar, M.; et al. Soil carbon sequestration potential in a Vertisol in central India-results from a 43-year long-term experiment and APSIM modeling. *Agric. Syst.* **2020**, *184*, 102906. [CrossRef]
21. Ochsner, T.E.; Cosh, M.H.; Cuenca, R.H.; Dorigo, W.A.; Draper, C.S.; Hagimoto, Y.; Kerr, Y.H.; Larson, K.M.; Njoku, E.G.; Small, E.E.; et al. State of the art in large-scale soil moisture monitoring. *Soil Sci. Soc. Am. J.* **2013**, *77*, 1888–1919. [CrossRef]
22. Dobriyal, P.; Qureshi, A.; Badola, R.; Hussain, S.A. A review of the methods available for estimating soil moisture and its implications for water resource management. *J. Hydrol.* **2012**, *458*, 110–117. [CrossRef]
23. Bogena, H.R.; Herbst, M.; Huisman, J.A.; Rosenbaum, U.; Weuthen, A.; Vereecken, H. Potential of wireless sensor networks for measuring soil water content variability. *Vadose Zone J.* **2010**, *9*, 1002–1013. [CrossRef]
24. Dorigo, W.A.; Wagner, W.; Hohensinn, R.; Hahn, S.; Paulik, C.; Xaver, A.; Gruber, A.; Drusch, M.; Mecklenburg, S.; van Oevelen, P.; et al. The International Soil Moisture Network: A data hosting facility for global in situ soil moisture measurements. *Hydrol. Earth Syst. Sci.* **2010**, *15*, 1675–1698. [CrossRef]
25. Entekhabi, D.; Reichle, R.H.; Koster, R.D.; Crow, W.T. Performance metrics for soil moisture retrieval and application requirements. *J. Hydrometeorol.* **2010**, *11*, 832–840. [CrossRef]
26. Kerr, Y.H.; Waldteufel, P.; Wigneron, J.P.; Delwart, S.; Cabot, F.; Boutin, J.; Escorihuela, M.J.; Font, J.; Reul, N.; Gruhier, C.; et al. The SMOS Mission: New Tool for Monitoring Key Elements of the Global Water Cycle. *Proc. IEEE* **2010**, *98900*, 666–687. [CrossRef]
27. Mohanty, M.; Sinha, N.K.; Patidar, R.K.; Somasundaram, J.; Chaudhary, R.S.; Hati, K.M.; Sammi Reddy, K.; Prabhakar, M.; Srinivas Rao, C.; Patra, A.K. Assessment of maize (*Zea mays* L.) productivity and yield gap analysis using simulation modelling in subtropical climate of central India. *J. Agrometeorol.* **2017**, *19*, 342–345. [CrossRef]
28. Wagner, W.; Hahn, S.; Figa, J.; Albergel, C.; de Rosnay, P.; Brocca, L.; Dorigo, W. Operations, challenges, and prospects of satellite-based surface soil moisture data services. In *Remote Sensing of Energy Fluxes and Soil Moisture Content*; Petropoulos, G.P., Ed.; CRC Press: Boca Raton, FL, USA, 2013; pp. 463–488.
29. Deng, M.; Meng, X.; Lu, Y.; Li, Z.; Zhao, L.; Hu, Z.; Chen, H.; Shang, L.; Wang, S.; LI, Q. Impact and sensitivity analysis of soil water and heat transfer parameterizations in Community Land Surface Model on the Tibetan Plateau. *J. Adv. Model. Earth Syst.* **2021**, *13*, e2021MS002670. [CrossRef]
30. Albergel, C.; de Rosnay, P.; Balsamo, G.; Isaksen, L.; Muñoz Sabater, J. Soil moisture analyses at ECMWF: Evaluation using global ground-based in situ observations. *J. Hydrometeorol.* **2021**, *13*, 1442–1460. [CrossRef]
31. Liao, K.; Liu, Y.; Zhu, Q. Spatio-temporal variation of near-surface soil water content in China from 1988 to 2016. *Soil Use Manag.* **2021**, *37*, 570–583. [CrossRef]
32. Sathyanadh, A.; Karipot, A.; Ranalkar, M.; Prabhakaran, T. Evaluation of soil moisture data products over Indian region and analysis of spatio-temporal characteristics with respect to monsoon rainfall. *J. Hydrol.* **2016**, *542*, 47–62. [CrossRef]
33. Agrawal, S.; Chakraborty, A. Evaluation of ESACCI satellite soil moisture product using in-situ CTCZ observations over India. *J. Earth Syst. Sci.* **2020**, *129*, 129. [CrossRef]

34. Albergel, C.; Dorigo, W.; Balsamo, G.; Muñoz-Sabater, J.; de Rosnay, P.; Isaksen, L.; Brocca, L.; De Jeu, R.; Wagner, W. Monitoring multi-decadal satellite earth observation of soil moisture products through land surface reanalyses. *Remote Sens. Environ.* **2013**, *138*, 77–89. [CrossRef]
35. Feng, H.; Zhang, M. Global land moisture trends: Drier in dry and wetter in wet over land. *Sci. Rep.* **2015**, *5*, 18018. [CrossRef] [PubMed]
36. Li, X.; Shao, M.; Jia, X.; Wei, X.; He, L. Depth persistence of the spatial pattern of soil-water storage along a small transect in the Loess Plateau of China. *J. Hydrol.* **2015**, *529*, 685–695. [CrossRef]
37. Qiu, J.; Gao, Q.; Wang, S.; Su, Z. Comparison of temporal trends from multiple soil moisture data sets and precipitation: The implication of irrigation on regional soil moisture trend. *Int. J. Appl. Earth Obs. Geoinf.* **2016**, *48*, 17–27. [CrossRef]
38. Almendra-Martín, L.; Martínez-Fernández, J.; Piles, M.; González-Zamora, Á.; Benito-Verdugo, P.; Gaona, J. Analysis of soil moisture trends in Europe using rank-based and empirical decomposition approaches. *Glob. Planet Chang.* **2022**, *215*, 103868. [CrossRef]
39. Khaliq, M.N.; Quarda, T.B.M.J.; Gachon, P.; Sushama, L.; St-Hilaire, A. Identification of hydrological trends in the presence of serial and cross correlations: A review of selected methods and their application to annual flow regimes of Canadian rivers. *J. Hydrol.* **2009**, *368*, 117–130. [CrossRef]
40. Huth, R.; Pokorn, L. Parametric versus non-parametric estimates of climatic trends. *Theor. Appl. Climatol.* **2004**, *77*, 107–112. [CrossRef]
41. Sen, P.K. Estimates of the regression coefficient based on Kendall's tau. *J. Am. Stat. Assoc.* **1968**, *63*, 1379–1389. [CrossRef]
42. Mann, H.B. Nonparametric tests against trend. *Econom. J. Econom. Soc.* **1945**, *13*, 245–259. [CrossRef]
43. Kendall, M.G. *Rank Correlation Methods*; Charles Griffin: London, UK, 1975; Volume 4.
44. Bandyopadhyay, A.; Bhadra, A.; Raghuwanshi, N.S.; Singh, R. Temporal trends in estimates of reference evapotranspiration over India. *J. Hydrol. Eng.* **2009**, *14*, 508–515. [CrossRef]
45. Subash, N.; RamMohan, H.S.; Sikka, A.K. Decadal frequency and trends of extreme excess/deficit rainfall during the monsoon season over different meteorological subdivisions of India. *J. Hydrol. Sci.* **2011**, *56*, 1090–1109. [CrossRef]
46. Berwal, P.; Murthy, C.S.; Raju, P.V.; Sesha Sai, M.V.R. Geospatial analysis of near-surface soil moisture time series data over Indian region. *Int. Arch. Photogramm. Remote Sens. Spat. Inf. Sci.* **2016**, *41*, 631–637. [CrossRef]
47. Agricoop, Department of Agriculture, Cooperation & Farmers Welfare, Ministry of Agriculture & Farmers Welfare Government. 2019. Available online: https://agridashboard.dac.gov.in/ (accessed on 30 June 2024).
48. Mujumdar, M.; Bhaskar, P.; Ramarao, M.V.S.; Uppara, U.; Goswami, M.; Borgaonkar, H.; Chakraborty, S.; Ram, S.; Mishra, V.; Rajeevan, M.; et al. Droughts and floods. In *Assessment of Climate Change over the Indian Region: A Report of the Ministry of Earth Sciences (MOES), Government of INDIA*; Springer Nature: Singapore, 2020; pp. 117–141.
49. Jain, R.; Kishore, P.; Singh, D.K. Irrigation in India: Status, challenges and options. *J. Soil Water Conserv.* **2019**, *18*, 354–363. [CrossRef]
50. GoI. *Agricultural Statistics at a Glance*; Government of India, Ministry of Agriculture & Farmers Welfare, Department of Agriculture & Farmers Welfare, Directorate of Economics & Statistics: New Delhi, India, 2021.
51. Gajbhiye, K.S.; Mandal, C. Agro-ecological zones, their soil resource and cropping systems. In *Status of Farm Mechanization in India, Cropping Systems, Status of Farm Mechanization in India*; NBSS&LUP: Nagpur, India, 2000; pp. 1–32.
52. Gruber, A.; Scanlon, T.; van der Schalie, R.; Wagner, W.; Dorigo, W. Evolution of the ESA CCI Soil Moisture climate data records and their underlying merging methodology. *Earth Syst. Sci. Data* **2019**, *11*, 717–739. [CrossRef]
53. Fang, L.; Hain, C.R.; Zhan, X.; Anderson, M.C. An inter-comparison of soil moisture data products from satellite remote sensing and a land surface model. *Int. J. Appl. Earth Obs. Geoinf.* **2016**, *48*, 37–50. [CrossRef]
54. McNally, A.; Shukla, S.; Arsenault, K.R.; Wang, S.; Peters-Lidard, C.D.; Verdin, J.P. Evaluating ESA CCI soil moisture in East Africa. *Int. J. Appl. Earth Obs. Geoinf.* **2016**, *48*, 96–109. [CrossRef]
55. Pai, D.S.; Sridhar, L.; Rajeevan, M.; Sreejith, O.P.; Satbhai, N.S.; Mukhopadhyay, B. Development of a new high spatial resolution ($0.25^\circ \times 0.25^\circ$) Long period (1901–2010) daily gridded rainfall data set over India and its comparison with existing data sets over the region. *Mausam* **2014**, *65*, 1–18. [CrossRef]
56. Srivastava, A.K.; Rajeevan, M.; Kshirsagar, S.R. Development of High Resolution Daily Gridded Temperature Data Set (1969–2005) for the Indian Region. *Atmos. Sci. Let.* **2009**, *10*, 249–254. [CrossRef]
57. Hadi, S.J.; Tombul, M. Long-term spatiotemporal trend analysis of precipitation and temperature over Turkey. *Meteorol. Appl.* **2018**, *25*, 445–455. [CrossRef]
58. Liou, Y.A.; Mulualem, G.M. Spatio–temporal assessment of drought in Ethiopia and the impact of recent intense droughts. *Remote Sens.* **2019**, *11*, 1828. [CrossRef]
59. Chauhan, A.S.; Singh, S.; Maurya, R.K.S.; Rani, A.; Danodia, A. Spatio-temporal trend analysis and future projections of precipitation at regional scale: A case study of Haryana, India. *J. Water Clim. Chang.* **2022**, *13*, 2143–2170. [CrossRef]
60. Guan, Y.; Gu, X.; Slater, L.J.; Li, J.; Kong, D.; Zhang, X. Spatio-temporal variations in global surface soil moisture based on multiple datasets: Intercomparison and climate drivers. *J. Hydrol.* **2023**, *625*, 130095. [CrossRef]
61. Rani, A.; Sehgal, V.K.; Dhakar, R.; Pragya; Sahoo, R.N.; Chakraborthy, D.; Kaur, R.; Manjaiah, K.; Marwaha, S. Spatio-temporal Analysis of Remote Sensing based Standardized Evaporative Drought Index during kharif Crop Season over India. *J. Agric. Phys.* **2023**, *23*, 132–143.
62. Hijmans, R.J.; Van Etten, J.; Cheng, J.; Mattiuzzi, M.; Sumner, M.; Greenberg, J.A.; Lamigueiro, O.P.; Bevan, A.; Racine, E.B.; Shortridge, A.; et al. Package 'raster'. *R Package* **2015**, *734*, 473.

63. McLeod, A.I.; McLeod, M.A. *Package 'Kendall'*; R Software: London, UK, 2015.
64. Pohlert, T.; Pohlert, M.T.; Kendall, S. Package 'trend'. In *Title Non-Parametric Trend Tests and Change-Point Detection*; R Software: London, UK, 2015.
65. Longobardi, A.; Villani, P. Trend analysis of annual and seasonal rainfall time series in the Mediterranean area. *Int. J. Clim.* **2010**, *30*, 1538–1546. [CrossRef]
66. Worku, T.; Khare, D.; Tripathi, S.K. Spatiotemporal trend analysis of rainfall and temperature, and its implications for crop production. *J. Water Clim. Chang.* **2019**, *10*, 799–817. [CrossRef]
67. Gadedjisso-Tossou, A.; Adjegan, K.I.; Kablan, A.K.M. Rainfall and temperature trend analysis by Mann–Kendall test and significance for Rainfed Cereal Yields in Northern Togo. *Science* **2021**, *3*, 17. [CrossRef]
68. Spearman, C. General intelligence objectively determined and measured. *Am. J. Psychol.* **1904**, *15*, 201–293. [CrossRef]
69. Wang, T.; Liu, Q.; Franz, T.E.; Li, R.; Lang, Y.; Fiebrich, C.A. Spatial patterns of soil moisture from two regional monitoring networks in the United States. *J. Hydrol.* **2017**, *552*, 578–585. [CrossRef]
70. Zhou, Q.; Sun, Z.; Liu, X.; Wei, X.; Peng, Z.; Yue, C.; Luo, Y. Temporal soil moisture variations in different vegetation cover types in karst areas of southwest China: A plot scale case study. *Water* **2019**, *11*, 1423. [CrossRef]
71. Pai, D.S.; Arti, B.; Sunitha, D.; Madhuri, M.; Badwaik, M.R.; Kundale, A.P.; Sulochana, G.; Mohapatra, M.; Rajeevan, M. Normal dates of onset/progress and withdrawal of southwest monsoon over India. *Mausam* **2020**, *71*, 553–570.
72. Rajeevan, M.; Unnikrishnan, C.K.; Bhate, J.; Niranjan Kumar, K.; Sreekala, P.P. Northeast monsoon over India: Variability and prediction. *Meteorol. Appl.* **2012**, *19*, 226–236. [CrossRef]
73. Laskar, A.H.; Ramesh, R.; Burman, J.; Midhun, M.; Yadava, M.G.; Jani, R.A.; Gandhi, N. Stable isotopic characterization of Nor'westers of southern Assam, NE India. *J. Clim. Chang.* **2015**, *1*, 75–87. [CrossRef]
74. Zheng, Y.; Bourassa, M.A.; Ali, M.M. The impact of rainfall on soil moisture variability in four homogeneous rainfall zones of India during strong, weak, and normal Indian summer monsoons. *Water* **2022**, *14*, 2788. [CrossRef]
75. Varikoden, H.; Revadekar, J.V. Relation between the rainfall and soil moisture during different phases of Indian monsoon. *Pure Appl. Geophys.* **2018**, *175*, 1187–1196. [CrossRef]
76. Guntu, R.K.; Agarwal, A. Spatiotemporal dependence of soil moisture and precipitation over India. *J. Hydrol.* **2022**, *610*, 127898.
77. Praveen, B.; Talukdar, S.; Shahfahad; Mahato, S.; Mondal, J.; Sharma, P.; Islam, A.R.M.T.; Rahman, A. Analyzing trend and forecasting of rainfall changes in India using non-parametrical and machine learning approaches. *Sci. Rep.* **2020**, *10*, 10342. [CrossRef]
78. Dhanagare, D.N. Drought in Maharashtra: Misplaced Priorities, Mismanagement of Water Resources. *Econ. Political Wkly.* **1992**, *27*, 1421–1425. Available online: http://www.jstor.org/stable/4398589 (accessed on 30 June 2024).
79. Shewale, M.P.; Kumar, S. Climatological features of drought incidences in India. In *Meteorological Monograph (Climatology 21/2005)*; National Climate Centre, Indian Meteorological Department: New Delhi, India, 2005.
80. *Manual for Drought Management*; Department of Agriculture, Cooperation and Farmers Welfare, Ministry of Agriculture and Farmers Welfare, Government of India: New Delhi, India, 2016.
81. Kumar, V.; Jain, S.K.; Singh, Y. Analysis of long-term rainfall trends in India. *Hydrol. Sci. J.* **2010**, *55*, 484–496. [CrossRef]
82. Guhathakurta, P.; Rajeevan, M. Trends in the rainfall pattern over India. *Int. J. Clim.* **2008**, *28*, 1453–1469. [CrossRef]
83. Singh, R.N.; Sah, S.; Das, B.; Potekar, S.; Chaudhary, A.; Pathak, H. Innovative trend analysis of spatio-temporal variations of rainfall in India during 1901–2019. *Theor. Appl. Climatol.* **2021**, *145*, 821–838. [CrossRef]
84. Oza, M.; Kishtawal, C.M. Trends in Rainfall and Temperature Patterns over North East India. *Earth Sci. India* **2014**, *7*, 90–105. [CrossRef]
85. Patle, G.T.; Libang, A. Trend analysis of annual and seasonal rainfall to climate variability in North-East region of India. *J. Nat. Appl. Sci.* **2014**, *6*, 480–483. [CrossRef]
86. Jaiswal, M.K.; Amin, N. The impact of land use dynamics on the soil erosion in the Panchnoi river basin, northeast India. *J. Geogr. Inst. Jovan Cvijic SASA* **2020**, *70*, 1–14. [CrossRef]
87. Marchang, R. *Changing Forest Land Use for Agriculture and Livelihood in North East India*; Working Paper (No. 523); Institute for Social and Economic Change: Karnataka, India, 2021.
88. Chevuturi, A.; Dimri, A.P.; Thayyen, R.J. Climate change over Leh (Ladakh), India. *Theor. Appl. Climatol.* **2018**, *131*, 531–545. [CrossRef]
89. Jain, S.K.; Kumar, V.; Saharia, M. Analysis of rainfall and temperature trends in northeast India. *Int. J. Clim.* **2013**, *33*, 968–978. [CrossRef]
90. Joiner, J.; Yoshida, Y.; Anderson, M.; Holmes, T.; Hain, C.; Reichle, R.; Koster, R.; Middleton, E.; Zeng, F.W. Global relationships among traditional reflectance vegetation indices (NDVI and NDII), evapotranspiration (ET), and soil moisture variability on weekly timescales. *Remote Sens. Environ.* **2018**, *219*, 339–352. [CrossRef] [PubMed]